

Dynamics of Black Hole Pairs I: Periodic Tables

Janna Levin^{*,1} and Becky Grossman^{**}

^{*}*Department of Physics and Astronomy, Barnard College of Columbia University, 3009 Broadway, New York, NY 10027*

¹*Institute for Strings, Cosmology and Astroparticle Physics, Columbia University, New York, NY 10027*

^{**}*Physics Department, Columbia University, New York, NY 10027*

janna@astro.columbia.edu and

becky@phys.columbia.edu

Although the orbits of comparable mass, spinning black holes seem to defy simple decoding, we find a means to decipher all such orbits. The dynamics is complicated by extreme perihelion precession compounded by spin-induced precession. We are able to quantitatively define and describe the fully three dimensional motion of comparable mass binaries with one black hole spinning and expose an underlying simplicity. To do so, we untangle the dynamics by capturing the motion in the orbital plane and explicitly separate out the precession of the plane itself. Our system is defined by the 3PN Hamiltonian plus spin-orbit coupling for one spinning black hole with a non-spinning companion. Our results are twofold: (1) We derive highly simplified equations of motion in a non-orthogonal orbital basis, and (2) we define a complete taxonomy for fully three-dimensional orbits. More than just a naming system, the taxonomy provides unambiguous and quantitative descriptions of the orbits, including a determination of the zoom-whirliness of any given orbit. Through a correspondence with the rationals, we are able to show that zoom-whirl behavior is prevalent in comparable mass binaries in the strong-field regime, as it is for extreme-mass-ratio binaries in the strong-field. A first significant conclusion that can be drawn from this analysis is that all generic orbits in the final stages of inspiral under gravitational radiation losses are characterized by precessing clovers with few leaves and that no orbit will behave like the tightly precessing ellipse of Mercury. The gravitational waveform produced by these low-leaf clovers will reflect the natural harmonics of the orbital basis – harmonics that, importantly, depend only on radius. The significance for gravitational wave astronomy will depend on the number of windings the pair executes in the strong-field regime and could be more conspicuous for intermediate mass pairs than for stellar mass pairs. The 3PN system studied provides an example of a general method that can be applied to any effective description of black hole pairs.

At first glance, the orbits of a black hole pair resist coherent description. Dynamically, black hole pairs involve non-linear relativistic effects leading to an extreme form of perihelion precession, coined zoom-whirl behavior, as well as spin precession that in turn drives orbits out of a plane. The three-dimensional precessions fill out a tangled path that shapes the gravitational waves both LIGO [1] and LISA [2] were designed to observe [3, 4, 5, 6, 7, 8, 9]. Despite appearances, we show the path can be untangled and a coherent description of fully three-dimensional precessing orbits proves entirely possible for one spinning black hole, one non-spinning.

The spacetime around two orbiting black holes eludes analytic description. While the impressive breakthroughs of numerical relativity [10, 11, 12, 13, 14, 15, 16] promise to resolve the final plunge of a black hole pair, computational expense relegates the majority of the inspiral to analytic methods. Several groups have gone to great pains to build a Hamiltonian formulation for two black holes in a Post-Newtonian (PN) approximation for analytic computation of orbits and the gravitational waves they generate. As a contribution to this great campaign, we use the conservative 3PN Hamiltonian plus spin-orbit couplings to deconstruct the full three-dimensional dynamics of black hole pairs, in the absence of radiation reaction. Our binaries are composed of one spinning black hole and one non-spinning black hole of any mass ratio.

The complicated three-dimensional motion can be beautifully decomposed into two-dimensional motion in an orbital plane with a precession of the orbital plane superposed [3]. Through this modular decomposition, we are able to define a complete taxonomy of all three-dimensional orbits in terms of orbits that are closed in the orbital plane. Further, we find the spectrum of orbits for a given black hole system. Importantly, the spectrum in the strong-field regime shows zoom-whirl behavior during which an orbit sweeps out to apastron and back in a zoom followed by a multiplicity of nearly circular whirls around the center of mass. It must be emphasized that our results prove zoom-whirl behavior is ubiquitous even for comparable mass binaries and unambiguously quantified in our taxonomy. Importantly, zoom-whirl motion has already been observed in numerical relativity [17].

From the outset, we acknowledge that the PN approximation is pushed to its breaking point in the strong-field regime where zoom-whirl behavior is most prevalent. However, the method we advocate – locating a periodic skeleton in an orbital basis – can be applied to any description of black hole binaries, including the effective one-body (EOB) approach [18] and extreme mass ratio inspirals (EMRIs) modeled by the Kerr spacetime [19]. Additionally, the closed-orbit taxonomy offers a new terrain for the comparison of the PN expansion to fully relativistic treatments [20, 21, 22]. Although quantita-

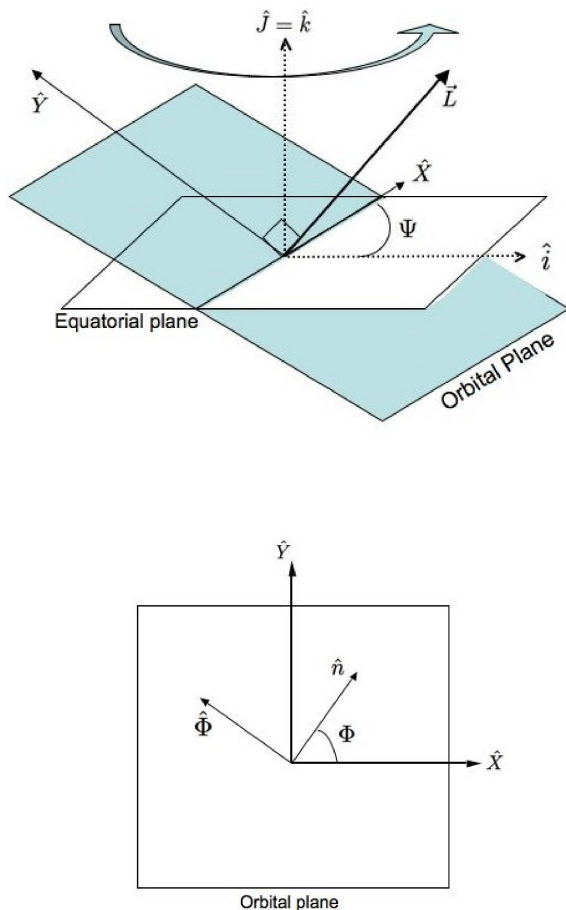


FIG. 1: Top: The orbital plane precesses around the $\hat{\mathbf{J}} = \hat{\mathbf{k}}$ axis through the angle Ψ . Bottom: The orbital plane can be spanned by the vectors $(\hat{\mathbf{X}}, \hat{\mathbf{Y}})$ or the vectors $(\hat{\mathbf{n}}, \hat{\Phi})$.

tive results will change in improved approximations, the qualitative features should be robust, as the detection of zoom-whirl behavior in fully relativistic numerical experiments implies [17].

I. PREVIEW

To provide the reader with a road map through intermediate results accumulated on our way to the periodic taxonomy, we preview some highlights here.

Our method can be broken into two main steps:

1. Simplified Equations of Motion. Since the perihelion precesses and the orbital plane precesses, the motion around a spinning black hole depends on angles as well as on the radius. In usual spherical coordinates, the equations of motion are quite complicated. By working in a non-orthogonal orbital basis, we show explicitly that the equations of motion are independent of (non-

orthogonal) angular variables.

Physically, we exploit the observation¹ that the orbit lies in the plane spanned by the coordinate \mathbf{r} and its canonical momentum \mathbf{p} ; that is, the orbital plane is perpendicular to the orbital angular momentum, $\mathbf{L} = \mathbf{r} \times \mathbf{p}$. The plane itself then precesses around the constant total angular momentum, \mathbf{J} . The importance of the orbital plane was clear in some of the earliest papers on spin-precession [3], although that early work generally imposed a quasi-circular restriction on the orbits. We decompose all motion into precession of the perihelion within the orbital plane with a precession of the entire plane superimposed, with no restrictions or approximations. A preview of the explicit construction is shown in Fig. 1. A fully precessing orbit is shown on the top in Fig. 2 while on the bottom the orbital plane traps a much simplified orbit, reminiscent of the equatorial orbits of Kerr black holes [19].

The simplified Hamilton's equations immediately inform us that all eccentric orbits have constant aphelia and perihelia.² When the aphelia and perihelia are one and the same, we have non-equatorial constant radius orbits, also known as spherical orbits (as previously found in [18, 28]). The spherical orbits are not necessarily periodic; they fill out a band on the surface of a sphere. They are nonetheless significant in our campaign to fully dissect the dynamics and are treated in a companion paper [29].

The simplified Hamilton's equations show that zoom-whirl patterns will be symmetric from one radial cycle to another when viewed in the orbital plane, as can be seen on the right of Fig. 2. A related subtle feature is that the three coordinate velocities in the orbital basis depend only on radius and are therefore periodic as an orbit executes a radial cycle from apastron to apastron. Taken together these symmetries in the orbital plane are intriguing for gravitational wave analysis. The waveforms must be decomposable into the orbital basis and therefore Fourier decomposable into the three fundamental frequencies that are the time average over one radial cycle of the instantaneous velocities. It remains to be seen how advantageous this might be for gravitational wave astronomy.

We restrict ourselves to completing the dynamical picture in this article since it is the dynamics that shapes the gravitational waves. In this spirit, step 1 above allows us to proceed to step 2:

2. Taxonomy of Fully 3D Orbits. We offer a method to completely taxonomize the dynamics with the restriction that only one of the black holes spins. Our approach includes *all* fully three-dimensional orbits de-

¹ The orbital plane is also emphasized in applications of PN dynamics to pulsar timing [23, 24, 25, 26].

² The constancy of periastron and apastron for every orbit might must have been implicitly understood in Refs. [18, 27].

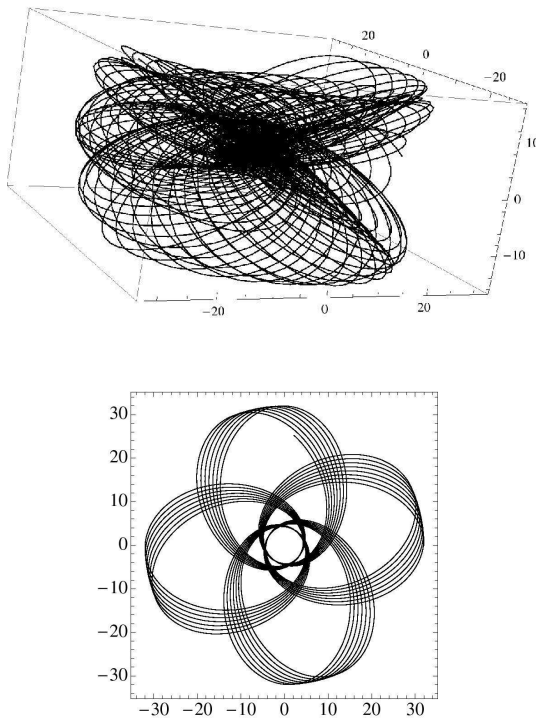


FIG. 2: Top: Fully three-dimensional orbit. Bottom: The trajectory as captured in the orbital plane.

scribed by the third-order Post-Newtonian (3PN) Hamiltonian plus spin-orbit couplings.

Our taxonomy extends the periodic tables for Kerr equatorial orbits [19] to fully non-equatorial orbits of comparable mass black hole binaries. In Ref. [19], we introduced a taxonomy for equatorial Kerr motion with the following salient features. Each entry in the Kerr periodic tables of Ref. [19] is a perfectly closed equatorial orbit identified by a rational number

$$q = w + \frac{v}{z} \quad (1)$$

where w counts the number of whirls, z counts the number of leaves, and v indicates the order in which the leaves are traced out. Since the rationals are dense on the number line, the periodics are dense in phase space. Consequently, *any* generic equatorial orbit can be *arbitrarily* well-approximated by a nearby periodic orbit. In this way, any generic orbit is approximately equivalent to a high-leaf orbit (high z). Additionally, any generic orbit can be approximated as a precession around a low-leaf orbit, a technique that might ultimately benefit signal extraction.

Our ambition in this paper is both to extend the taxonomy to comparable mass binaries and to resolve the non-equatorial motion of spinning binaries. Truly periodic three-dimensional motion follows when the trajectory closes in the orbital plane *and* the precession of the

entire plane closes simultaneously. Fully closed motion requires two rationals, each representing a ratio of fundamental frequencies. And although in principle there must exist orbits that are fully periodic in the three-dimensional motion – as Poincaré argued [30] – our taxonomy of bound orbits needs only the weaker condition of periodicity in the orbital plane. Not every orbit that is closed in the orbital plane will be closed in the full three-dimensional space. In other words, for the less restrictive condition of orbital plane periodicity we only need one rational ratio of frequencies. As will be explained in detail in §III, the aperiodic orbit of Fig. 2 can be approximated as a precession around a 4-leaf clover in the orbital plane.

Although the PN approximation is poor in the strong-field, the qualitative results should survive a full relativistic treatment. Spin-spin couplings will impose additional modulations on the orbital plane picture but since spin-spin couplings are higher-order in the PN expansion, the expectation has been that their effect can be treated as a perturbation [28]. In a companion paper we will argue that although a small perturbation, the spin-spin couplings are responsible for the emergence of chaos around unstable orbits [29].

We emphasize that for real spinning astrophysical black holes, the orbits we resolve in this paper are not an exotic subset of orbits, but rather are descriptive of *all* bound orbits – *all* non-circular orbits are captured in the spectrum of rationals. There is a long-standing argument that black hole binaries will circularize by the time they enter the bandwidth of the gravitational wave observatories. However this is not possible for spinning black holes. Circular orbits *do not exist* for misaligned spins. Although spherical orbits do exist, they are destroyed by the spin-spin effects [29]. What’s more, black hole pairs formed in dense clusters are not expected to circularize by the time of merger and are expected to be plentiful sources for advanced LIGO [31] While we restrict ourselves to one spinning black hole and one non-spinning in this paper, the scenario is both astrophysically possible in its own right and theoretically important to lay the foundation for the two spinning case with spin-spin included, a task we return to in a companion paper [29]

We express Hamilton’s equations in a non-orthogonal orbital basis in §II. We discuss the closed orbit taxonomy in §III. In §IV, we show periodic tables for two different black hole binaries, a comparable mass binary and a non-spinning extreme mass ratio pair. Appendix §A details the projection of Hamilton’s equations onto our orbital basis. In the conclusions, §V, we discuss the modulations predicted from spin-spin couplings and those imposed by spinning both black holes.

II. HAMILTON’S EQUATIONS OF MOTION IN THE ORBITAL BASIS

The culmination of this section will be the compact form of the equations of motion (Eqs. (28)) in a non-

orthonormal orbital basis. To get there will require a few short subsections. We begin with the 3PN Hamiltonian including spin-orbit couplings.

A. The 3PN Hamiltonian + Spin-Orbit Couplings

Although the 3PN Hamiltonian is nearly a page long, the Hamiltonian formulation of black hole pairs has certain advantages over the Kerr fully relativistic description of test particle motion around a single black hole. Most notable in this context, the ADM-Hamiltonian effectively describes center of mass motion in flat space. This will allow us to manipulate spatial vectors at will and locate the orbital plane. (This work has suggested a means to generalize to the fully relativistic Kerr system.

That research is in progress.)

To begin, take the 3PN Hamiltonian including spin-orbit coupling as it is conventionally written in dimensionless coordinates. If \mathcal{R} is the ADM coordinate vector and \mathcal{P} is the ADM momentum vector, then the dimensionless center-of-mass coordinate vector is $\mathbf{r} = \mathcal{R}/M$ and its canonical momentum is $\mathbf{p} = \mathcal{P}/\mu$ where the total mass is $M = m_1 + m_2$ for a pair with black hole masses m_1 and m_2 and the reduced mass is $\mu = m_1 m_2 / M$ with the dimensionless combination $\eta = \mu / M$. All vector quantities will always be in bold so that r is to be understood as the magnitude $r = \sqrt{\mathbf{r} \cdot \mathbf{r}}$. Unit vectors such as $\hat{\mathbf{n}} = \mathbf{r}/r$ will additionally carry a hat as well as being bold. The dimensionless reduced Hamiltonian $H = \mathcal{H}/\mu$, where \mathcal{H} is the physical Hamiltonian, can be written to 3PN order as [32, 33, 34, 35, 36, 37]

$$H = H_{PN} + H_{SO} \quad , \quad (2)$$

where

$$H_{PN} = H_N + H_{1PN} + H_{2PN} + H_{3PN} \quad (3)$$

$$\begin{aligned} H_N &= \frac{\mathbf{p}^2}{2} - \frac{1}{r} \\ H_{1PN} &= \frac{1}{8} (3\eta - 1) (\mathbf{p}^2)^2 - \frac{1}{2} [(3 + \eta) \mathbf{p}^2 + \eta(\hat{\mathbf{n}} \cdot \mathbf{p})^2] \frac{1}{r} + \frac{1}{2r^2} \\ H_{2PN} &= \frac{1}{16} (1 - 5\eta + 5\eta^2) (\mathbf{p}^2)^3 + \frac{1}{8} [(5 - 20\eta - 3\eta^2) (\mathbf{p}^2)^2 \\ &\quad - 2\eta^2(\hat{\mathbf{n}} \cdot \mathbf{p})^2 \mathbf{p}^2 - 3\eta^2(\hat{\mathbf{n}} \cdot \mathbf{p})^4] \frac{1}{r} \\ &\quad + \frac{1}{2} [(5 + 8\eta) \mathbf{p}^2 + 3\eta(\hat{\mathbf{n}} \cdot \mathbf{p})^2] \frac{1}{r^2} - \frac{1}{4} (1 + 3\eta) \frac{1}{r^3} \end{aligned} \quad (4)$$

$$\begin{aligned} H_{3PN} &= \frac{1}{128} (-5 + 35\eta - 70\eta^2 + 35\eta^3) (\mathbf{p}^2)^4 + \frac{1}{16} [(-7 + 42\eta - 53\eta^2 - 5\eta^3) (\mathbf{p}^2)^3 \\ &\quad + (2 - 3\eta)\eta^2(\hat{\mathbf{n}} \cdot \mathbf{p})^2(\mathbf{p}^2)^2 + 3(1 - \eta)\eta^2(\hat{\mathbf{n}} \cdot \mathbf{p})^4 \mathbf{p}^2 - 5\eta^3(\hat{\mathbf{n}} \cdot \mathbf{p})^6] \frac{1}{r} \\ &\quad + \left[\frac{1}{16} (-27 + 136\eta + 109\eta^2) (\mathbf{p}^2)^2 + \frac{1}{16} (17 + 30\eta)\eta(\hat{\mathbf{n}} \cdot \mathbf{p})^2 \mathbf{p}^2 + \frac{1}{12} (5 + 43\eta)\eta(\hat{\mathbf{n}} \cdot \mathbf{p})^4 \right] \frac{1}{r^2} \\ &\quad + \left\{ \frac{1}{192} [-600 + (3\pi^2 - 1340)\eta - 552\eta^2] \mathbf{p}^2 - \frac{1}{64} (340 + 3\pi^2 + 112\eta)\eta(\hat{\mathbf{n}} \cdot \mathbf{p})^2 \right\} \frac{1}{r^3} \\ &\quad + \frac{1}{96} [12 + (872 - 63\pi^2)\eta] \frac{1}{r^4} \quad . \end{aligned} \quad (5)$$

The reduced spin-orbit Hamiltonian is

$$H_{SO} = \delta_1 \frac{\mathbf{L} \cdot \mathbf{S}}{r^3} \quad (6)$$

where in this paper, we restrict our analysis to only one

spinning body with reduced spin

$$\mathbf{S} = \mathbf{a}(m_1^2/\mu M) \quad , \quad (7)$$

mass m_1 , and

$$\delta_1 \equiv \left(2 + \frac{3m_2}{2m_1}\right) \eta \quad . \quad (8)$$

Physical values of the dimensionless spin amplitude range over $0 \leq a \leq 1$. In a companion paper, we will generalize to two spinning bodies [29]. We omit spin-spin coupling terms. The reduced orbital angular momentum is

$$\mathbf{L} = \mathbf{r} \times \mathbf{p} \quad . \quad (9)$$

Notice that with units included, the physical orbital angular momentum is $\mathbf{L}\mu M$.

The equations of motion are given by

$$\dot{\mathbf{r}} = \frac{\partial H}{\partial \mathbf{p}} \quad , \quad \dot{\mathbf{p}} = -\frac{\partial H}{\partial \mathbf{r}} \quad (10)$$

and the evolution equation for the spins and the angular momentum can be found from the Poisson brackets:

$$\begin{aligned} \dot{\mathbf{S}} &= \{\mathbf{S}, H\} = \frac{\partial H}{\partial \mathbf{S}} \times \mathbf{S} \\ \dot{\mathbf{L}} &= \{\mathbf{L}, H\} = \frac{\partial H}{\partial \mathbf{L}} \times \mathbf{L} \end{aligned} \quad (11)$$

which comes to

$$\begin{aligned} \dot{\mathbf{S}} &= \delta_1 \frac{\mathbf{L} \times \mathbf{S}}{r^3} \\ \dot{\mathbf{L}} &= \delta_1 \frac{\mathbf{S} \times \mathbf{L}}{r^3} \quad . \end{aligned} \quad (12)$$

B. Conserved Quantities

It is well-known that this system has many useful conserved quantities.³ The Hamiltonian is conserved by construction. The conservation of total angular momentum follows from Eqs. (12)

$$\mathbf{J} = \mathbf{L} + \mathbf{S} \quad . \quad (13)$$

Also conserved are the magnitude of S and L , as can be confirmed by taking the dot-products with Eqs. (12):

$$\begin{aligned} \mathbf{S} \cdot \dot{\mathbf{S}} &= \frac{1}{2} \frac{d}{dt} (S^2) \propto \mathbf{L} \cdot (\mathbf{S} \times \mathbf{L}) = 0 \\ \mathbf{L} \cdot \dot{\mathbf{L}} &= \frac{1}{2} \frac{d}{dt} (L^2) \propto \mathbf{S} \cdot (\mathbf{L} \times \mathbf{S}) = 0 \end{aligned} \quad (14)$$

³ Although it is by now well-confirmed that there is chaos when the black holes spin [27, 38, 39, 40, 41, 42, 43, 44], we are dealing with a restricted situation of only one body spinning in the Hamiltonian formulation and our orbits are not chaotic to this order in the approximation [45]. This is not in conflict with earlier work on chaos in the Lagrangian approximation [46]. At higher order including spin-spin couplings, a pair of spinning black holes loses constants of the motion opening a window for chaotic motion [29].

Finally, the component of \mathbf{L} in the \mathbf{J} direction must be conserved as can be seen from

$$\begin{aligned} \dot{\mathbf{L}} &= \delta_1 \frac{\mathbf{S} \times \mathbf{L}}{r^3} \\ &= \delta_1 \frac{\mathbf{J} \times \mathbf{L}}{r^3} \end{aligned} \quad (15)$$

from which it follows that the change in \mathbf{L} is always perpendicular to \mathbf{J} .

C. The equations of motion

We want to express the equations of motion derived from Eq. (10) in the following form:

$$\begin{aligned} \dot{\mathbf{r}} &= A\mathbf{p} + B\hat{\mathbf{n}} + \text{spin pieces} \\ \dot{\mathbf{p}} &= C\mathbf{p} + D\hat{\mathbf{n}} + \text{spin pieces} \quad . \end{aligned} \quad (16)$$

This form helps consolidate the equations of motion before we project from the vector equations to component equations in the next section (§IID). We need to identify the functions A, B, C, D in terms of derivatives on the Hamiltonian, which can be thought of as a function of $(r, \mathbf{p}, (\hat{\mathbf{n}} \cdot \mathbf{p}))$. Considering the non-spinning piece, H_{PN} first, we break up the partial derivatives on the right hand side of Hamilton's equations in the following way,

$$\left. \frac{\partial H_{PN}}{\partial \mathbf{p}} \right|_{\mathbf{r}} = \left. \frac{\partial H_{PN}}{\partial \mathbf{p}^2} \right|_{r, (\hat{\mathbf{n}} \cdot \mathbf{p})} \frac{\partial \mathbf{p}^2}{\partial \mathbf{p}} + \left. \frac{\partial H_{PN}}{\partial (\hat{\mathbf{n}} \cdot \mathbf{p})} \right|_{r, \mathbf{p}} \frac{\partial (\hat{\mathbf{n}} \cdot \mathbf{p})}{\partial \mathbf{p}}$$

and

$$-\left. \frac{\partial H_{PN}}{\partial \mathbf{r}} \right|_{\mathbf{p}} = -\left. \frac{\partial H_{PN}}{\partial (\hat{\mathbf{n}} \cdot \mathbf{p})} \right|_{r, \mathbf{p}} \frac{\partial (\hat{\mathbf{n}} \cdot \mathbf{p})}{\partial \hat{\mathbf{n}}} \frac{\partial \hat{\mathbf{n}}}{\partial \mathbf{r}} - \left. \frac{\partial H_{PN}}{\partial r} \right|_{\mathbf{p}, (\hat{\mathbf{n}} \cdot \mathbf{p})} \frac{\partial r}{\partial \mathbf{r}}$$

where we are careful to indicate the quantities held fixed in each term. Using

$$\frac{\partial (\hat{\mathbf{n}} \cdot \mathbf{p})}{\partial \hat{\mathbf{n}}} \frac{\partial \hat{\mathbf{n}}}{\partial \mathbf{r}} = \frac{\mathbf{p}}{r} - \frac{(\hat{\mathbf{n}} \cdot \mathbf{p})}{r} \hat{\mathbf{n}} \quad (17)$$

we define

$$A \equiv 2 \left. \frac{\partial H_{PN}}{\partial \mathbf{p}^2} \right|_{r, (\hat{\mathbf{n}} \cdot \mathbf{p})} \quad (18)$$

$$B \equiv \left. \frac{\partial H_{PN}}{\partial (\hat{\mathbf{n}} \cdot \mathbf{p})} \right|_{r, \mathbf{p}}$$

$$C \equiv -\frac{1}{r} \left. \frac{\partial H_{PN}}{\partial (\hat{\mathbf{n}} \cdot \mathbf{p})} \right|_{r, \mathbf{p}} = -\frac{B}{r}$$

$$\begin{aligned} D &\equiv -\left. \frac{\partial H_{PN}}{\partial r} \right|_{\mathbf{p}, (\hat{\mathbf{n}} \cdot \mathbf{p})} + \left. \frac{\partial H_{PN}}{\partial (\hat{\mathbf{n}} \cdot \mathbf{p})} \right|_{r, \mathbf{p}} \frac{(\hat{\mathbf{n}} \cdot \mathbf{p})}{r} \\ &= -\left. \frac{\partial H_{PN}}{\partial r} \right|_{\mathbf{p}, (\hat{\mathbf{n}} \cdot \mathbf{p})} - (\hat{\mathbf{n}} \cdot \mathbf{p})C \quad . \end{aligned} \quad (19)$$

The variations of the spinning piece of the Hamiltonian are simply

$$\begin{aligned} \frac{\partial H_{SO}}{\partial \mathbf{p}} &= \delta_1 \frac{\mathbf{S} \times \mathbf{r}}{r^3} \\ -\frac{\partial H_{SO}}{\partial \mathbf{r}} &= -\delta_1 \frac{\mathbf{p} \times \mathbf{S}}{r^3} + 3\delta_1 \frac{\mathbf{L} \cdot \mathbf{S}}{r^4} \hat{\mathbf{n}} \quad . \end{aligned} \quad (20)$$

With these definitions, and making use of $-\mathbf{p} \times \mathbf{S} = \mathbf{S} \times \mathbf{p}$, we can write the vector equations of motion compactly as

$$\begin{aligned} \dot{\mathbf{r}} &= A\mathbf{p} + B\hat{\mathbf{n}} + \delta_1 \frac{\mathbf{S} \times \mathbf{r}}{r^3} \\ \dot{\mathbf{p}} &= C\mathbf{p} + D\hat{\mathbf{n}} + \delta_1 \frac{\mathbf{S} \times \mathbf{p}}{r^3} + 3\delta_1 \frac{\mathbf{L} \cdot \mathbf{S}}{r^4} \hat{\mathbf{n}} \quad . \end{aligned} \quad (21)$$

To go from these vector equations to component form requires we choose a basis. In the next section we will build the orbital basis of Fig. 1, and cast Eqs. (21) in component form.

D. The Orbital Basis

The clarity of the form of the equations of motion depends on the basis used to express them. There are several choices although the one we are calling the orbital basis leads to profound clarity of expression. We will build a *non*-orthogonal, unit normalized basis $(\hat{\mathbf{n}}, \hat{\Phi}, \hat{\Psi})$ in this section.

There are two special planes to consider when spin precession drives three-dimensional orbits. There is the orbital plane, which is the plane perpendicular to \mathbf{L} , and there is the equatorial plane, which is the plane perpendicular to \mathbf{J} (see Fig. 1). We will find an orthonormal basis that spans the orbital plane and then add the motion of the plane itself, which will be in a direction that is not orthogonal to the orbital plane. The technique of moving into an orbital plane and projecting equations of motion onto this basis is familiar from celestial mechanics and has seen application in the PN approximation to binary pulsars [23, 24, 25, 26]. We depart from the usual approach by adopting a non-orthogonal basis.

The vectors $\hat{\mathbf{n}}$ and \mathbf{p} lie in the orbital plane by the definition $\mathbf{L} = r\hat{\mathbf{n}} \times \mathbf{p}$. We can also span the orbital plane by orthonormal vectors $(\hat{\mathbf{n}}, \hat{\Phi})$ where

$$\hat{\Phi} = \hat{\mathbf{L}} \times \hat{\mathbf{n}} \quad . \quad (22)$$

We will work in terms of $(\hat{\mathbf{n}}, \hat{\Phi})$ when considering motion in the orbital plane.

To separate out the precession of the orbital plane from the three-dimensional motion, another basis will be useful for intermediate steps. The $(\hat{\mathbf{X}}, \hat{\mathbf{Y}})$ basis spans the orbital plane but rotates with the precession of \mathbf{L} :

$$\begin{aligned} \hat{\mathbf{X}} &= \frac{\hat{\mathbf{J}} \times \hat{\mathbf{L}}}{\sin \theta_L} \\ \hat{\mathbf{Y}} &= \hat{\mathbf{L}} \times \hat{\mathbf{X}} \quad , \end{aligned} \quad (23)$$

where $\theta_L = \arccos(\hat{\mathbf{L}} \cdot \hat{\mathbf{J}})$ is constant. The $\hat{\mathbf{X}}$ axis is orthogonal to both $\hat{\mathbf{J}}$ and $\hat{\mathbf{L}}$ by construction and so lies on the intersection of the orbital plane and the equatorial plane. The entire orbital plane maintains a fixed angle $\theta_Y = \pi/2 - \theta_L$ with \mathbf{J} as it precesses with the precession of \mathbf{L} . The motion of the orbital plane can be understood as the motion of $\hat{\mathbf{X}}$ in the equatorial plane through an angle Ψ where

$$\hat{\Psi} = \hat{\mathbf{J}} \times \hat{\mathbf{X}} \quad . \quad (24)$$

Let $\hat{\mathbf{J}} = \hat{\mathbf{k}}$ and let the unit vectors $\hat{\mathbf{i}}$ and $\hat{\mathbf{j}}$ span the equatorial plane. The speed of Ψ motion can then be determined:

$$\cos \dot{\Psi} = \dot{\hat{\mathbf{X}}} \cdot \hat{\mathbf{i}} = \frac{(\hat{\mathbf{J}} \times \dot{\hat{\mathbf{L}}}) \cdot \hat{\mathbf{i}}}{L \sin \theta_L} = \Omega_L \hat{\Psi} \cdot \hat{\mathbf{i}} = -\Omega_L \sin \Psi, \quad (25)$$

where we have explicitly used the constancy of the magnitude L . From this we conclude

$$\Omega_L = \dot{\Psi} = \delta_1 \frac{J}{r^3} \quad . \quad (26)$$

does not depend on any angles.

To find our simplified equations of motion we work in the non-orthogonal, unit normalized basis $(\hat{\mathbf{n}}, \hat{\Phi}, \hat{\Psi})$ in the next section.

E. Final equations of motion in the orbital plane

The four equations of motion in the orbital plane are obtained by projecting Hamilton's equations onto the basis vectors $(\hat{\mathbf{n}}, \hat{\Phi})$. We do this explicitly in appendix §A, where the projections onto the orbital basis vectors generate the four equations,

$$\begin{aligned} \dot{\mathbf{r}} \cdot \hat{\mathbf{n}} &= \frac{\partial H}{\partial \mathbf{p}} \cdot \hat{\mathbf{n}} \\ \dot{\mathbf{r}} \cdot \hat{\Phi} &= \frac{\partial H}{\partial \mathbf{p}} \cdot \hat{\Phi} \\ \dot{\mathbf{p}} \cdot \hat{\mathbf{n}} &= -\frac{\partial H}{\partial \mathbf{r}} \cdot \hat{\mathbf{n}} \\ \dot{\mathbf{p}} \cdot \hat{\Phi} &= -\frac{\partial H}{\partial \mathbf{r}} \cdot \hat{\Phi} \quad . \end{aligned} \quad (27)$$

Compiling the equations of appendix §A concisely gives the remarkably simple equations of motion in the orbital plane coordinates (r, Φ) and their canonical momenta (P_r, P_Φ) ,

$$\boxed{\begin{aligned} \dot{r} &= AP_r + B, & \dot{P}_r &= A\frac{L^2}{r^3} - \frac{B}{r}P_r + D + 3\delta_1\frac{\mathbf{S}\cdot\mathbf{L}}{r^4} \\ \dot{\Phi} &= A\frac{L}{r^2} - \frac{L}{J}\Omega_L, & \dot{P}_\Phi &= 0 \end{aligned}} \quad (28)$$

where $P_\Phi = L$. The orbital plane precesses at a rate that depends only on r , as calculated in the previous section (§IID):

$$\dot{\Psi} = \Omega_L = \delta_1\frac{J}{r^3}, \quad \dot{P}_\Psi = 0 \quad (29)$$

with $\delta_1 \equiv \left(2 + \frac{3m_2}{2m_1}\right)\eta$ and $P_\Psi = L_z$. For completeness, we can track the precessions of the spin and the angular momentum:

$$\begin{aligned} \dot{\mathbf{S}} &= \Omega_L \hat{\mathbf{J}} \times \mathbf{S} \\ \dot{\mathbf{L}} &= \Omega_L \hat{\mathbf{J}} \times \mathbf{L} \end{aligned} \quad (30)$$

As noted earlier, $\mathbf{S}\cdot\mathbf{L} = \text{constant}$. Notice, this basis is explicitly constructed for $\mathbf{S}\times\mathbf{L} \neq 0$. When the spin and orbital angular momentum are aligned, anti-aligned, or spin is zero, then motion is confined to a plane and we should use the usual equatorial planar basis. This is done explicitly in §IVB.

The functions A, B, C, D of Eqs. (19) depend only on r, P_r and constants. This can be seen by noting that A, B, C, D are functions of $(r, (\hat{\mathbf{n}}\cdot\mathbf{p}), \mathbf{p}^2)$. Now, \mathbf{p} can be written in terms of a piece in the radial direction and a piece perpendicular to the radial direction:

$$\begin{aligned} \mathbf{p} &= (\mathbf{p}\cdot\hat{\mathbf{n}})\hat{\mathbf{n}} + (\hat{\mathbf{n}}\times\mathbf{p})\times\hat{\mathbf{n}} \\ &= P_r\hat{\mathbf{n}} + \frac{\mathbf{L}}{r}\times\hat{\mathbf{n}} \end{aligned} \quad (31)$$

so that

$$\mathbf{p}^2 = P_r^2 + \frac{L^2}{r^2} \quad (32)$$

and L equals a constant. The term \mathbf{p}^2 can therefore be expressed as a function of (r, P_r) only. Meanwhile, $(\hat{\mathbf{n}}\cdot\mathbf{p}) = P_r$ and so any function of $(r, (\hat{\mathbf{n}}\cdot\mathbf{p}), \mathbf{p}^2)$ is equally well a function only of (r, P_r) and constants.

Consequently, the above equations of motion are, amazingly enough, independent⁴ of the angles (Φ, Ψ) .

The purely radial dependence of the equations of motion immediately informs us of four crucial facts (valid to this order in the PN approximation):

1. *There are constant radius orbits.* These were already found in Ref. [18, 28] and drop out particularly simply in the orbital basis. In the equatorial plane these are of course the usual circular orbits. Out of the equatorial plane they have been called spherical orbits in the literature since the orbits trace out an annulus on the surface of a sphere. We will continue in this spirit and call them spherical orbits, or, more exactly, constant radius orbits. To see that they exist, notice that the spherical orbits correspond to solutions of $\dot{r} = \dot{P}_r = 0$ and these roots – according to Eqs. (28) – can only depend on constants $(m_1/m_2, S, L, \theta_{LS})$, not on angles. In fact, we have a pseudo effective-potential description as we explain in the next section.

2. *All eccentric orbits have constant apastra and perihelia.* Similar to the reasoning above, the solutions to the condition $P_r = 0$ are the turning points⁵ and thus are the apastron and perihelion of any orbit. These values can depend only on constants [29].

3. *The orbital angle and precessional angle swept out between successive apastra are constant.* The angles swept out as an orbit moves from one apastron to another are simply given by

$$\begin{aligned} \Delta\Phi &= 2\int_{r_a}^{r_p}\frac{\dot{\Phi}}{r}dr \\ \Delta\Psi &= 2\int_{r_a}^{r_p}\frac{\dot{\Psi}}{r}dr \end{aligned} \quad (33)$$

and depend only on constants.

4. *All three coordinate velocities are periodic in r .* The three coordinate velocities in the orbital basis

$$\dot{r}, \quad \dot{\Phi}, \quad \text{and} \quad \dot{\Psi}, \quad (34)$$

depend only on the variable r (or $P_r(r)$) and thereby inherit r 's periodicity. They can be averaged over one radial cycle to define three fundamental frequencies

$$\omega_r = \frac{2\pi}{T_r}, \quad \omega_\Phi, \quad \text{and} \quad \omega_\Psi \quad (35)$$

⁴ The simplicity of the orbital equations of motion can of course be recast in terms of symmetries. Rotations about $\hat{\mathbf{L}}$ through the angle Φ , $R_{\hat{\mathbf{L}}}(\Phi)$, and rotations about $\hat{\mathbf{J}}$ through the angle Ψ , $R_{\hat{\mathbf{J}}}(\Psi)$, leave the dynamics invariant. The coordinates Φ and Ψ are cyclic and $\dot{P}_\Phi = \dot{P}_\Psi = 0$. The symmetries correspond to conserved L and L_z with $P_\Phi = L$ and $P_\Psi = L_z$.

⁵ When $P_r = 0$, $B = 0$ and so $\dot{r} = AP_r + B = 0$. Therefore we take the $\dot{r} = 0$ condition to be synonymous with $P_r = 0$.

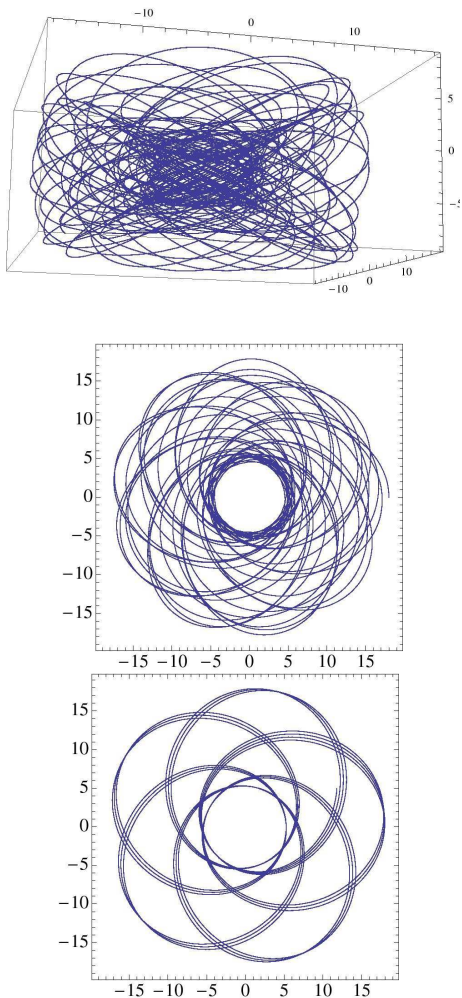


FIG. 3: A generic orbit in the strong-field. The initial conditions are $m_2/m_1 = \frac{1}{4}$, $L = 3.5$, $\theta_{LS} = \frac{\pi}{3}$, $a = 0.9$, and $r_i = 18$. Top: The full three-dimensional orbit. Middle: A projection of the full orbit onto the equatorial plane. Looking closely, the angle swept out from leaf to leaf is not the same under this projection. Bottom: The orbit as caught by the orbital plane. The angle swept out in the orbital plane from leaf to leaf is always the same. Further, the constancy of the apastron is clear.

where T_r is the radial period from apastron to apastron (We will define ω_Φ and ω_Ψ a bit later in Eqs. (36) and (41)).⁶

The powerful simplicity of the description in the orbital basis is visually manifest in Fig. 3. The figure shows a fully three-dimensional, generic orbit on the top. The lowest panel is the same snapshot captured in the orbital plane. Notice how the orbital plane reveals the con-

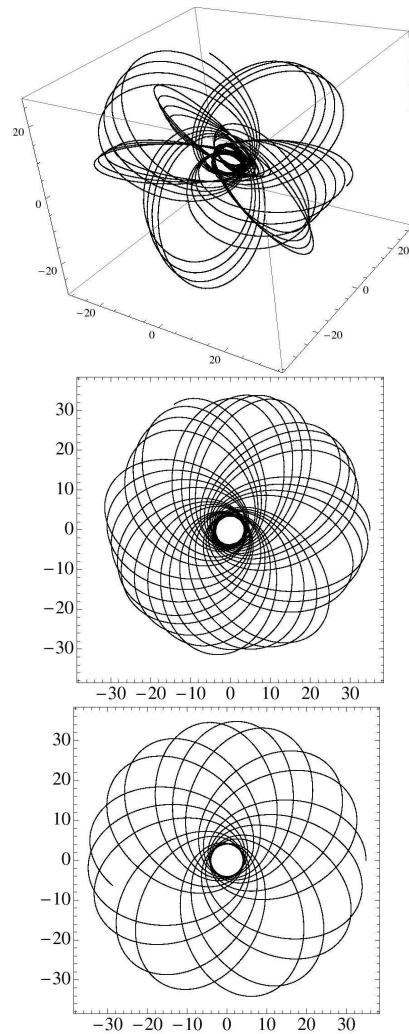


FIG. 4: The initial conditions are $m_2/m_1 = \frac{1}{4}$, $L = 3.5$, $\theta_{LS} = \frac{\pi}{3}$, $a = 0.9$ and $E = -0.023548373360051289666$. Top: The full orbit. Middle: A projection on the equatorial plane. Bottom: The orbit as it appears in the orbital plane

stancy of the three-dimensional apastron and perihelion as claimed in point 2 above. Also notice that the spacing between leaves is always symmetric in the orbital plane. Said another way, the angle swept out in the orbital plane between apastra is always the same, as claimed in point 3. Neither of these features is apparent from the fully three-dimensional snapshot or from the projection onto the *equatorial* plane shown in the middle view. Another generic orbit is shown in Fig. 4.

The four facts above have two significant implications:

- A gravitational waveform can be Fourier decomposed in the three fundamental frequencies of Eq. (34).
- There should be a spectrum of orbits that are closed in the orbital plane, and that spectrum must have a correspondence with the rationals. We can therefore generalize the Kerr taxonomy of Ref. [19] to non-equatorial orbits of comparable mass black hole binaries.

⁶ Points 1 and 2 are also true for Kerr non-equatorial orbits, although 3 and 4 are not.

We complete the dynamical picture by moving on to the periodic taxonomy for black hole binaries.

III. CLOSED ORBIT TAXONOMY

Any dynamical study benefits from locating the closed orbits – orbits that return to their initial values after some finite period. Poincaré was the first to realize that periodic orbits structure the entire dynamics [30]. Although a set of measure zero, the periodic orbits are dense in phase space. Consequently, any orbit can be approximated as near some periodic orbit. In that sense, the periodic set forms the skeleton of the dynamics. What's more, they are all one needs to know since to arbitrary precision even an aperiodic generic orbit is arbitrarily close to some periodic orbit, though possibly one with very high period.

The periodic set corresponds to a spectrum of rational numbers. That spectrum of rationals shows that the zoom-whirl behavior known for extreme-mass-ratio binaries is prevalent in the strong-field regime of comparable binaries as well. Zoom-whirl behavior is therefore not exotic but rather the norm for the strong-field. The spectrum of rationals renders the zoom-whirl behavior of any orbit quantifiable and unambiguous.

Consider the coordinate velocities of Eq. (34). Taking the time average of the Φ -frequency over one radial cycle gives the fundamental frequency

$$\omega_\Phi = \frac{2}{T_r} \int_{r_a}^{r_p} \frac{\dot{\Phi}}{\dot{r}} dr = \frac{\Delta\Phi}{T_r} = \omega_r \frac{\Delta\Phi}{2\pi} , \quad (36)$$

so that

$$\frac{\omega_\Phi}{\omega_r} = \frac{\Delta\Phi}{2\pi} . \quad (37)$$

An orbit that is closed in the orbital plane has rationally related frequencies

$$\frac{\omega_\Phi}{\omega_r} = 1 + q_\Phi . \quad (38)$$

By Eq. (37), we can interpret the rational in terms of the angle swept out from leaf to leaf in the orbital plane

$$\frac{\Delta\Phi}{2\pi} = 1 + q_\Phi = 1 + w_\Phi + \frac{v_\Phi}{z_\Phi} , \quad (39)$$

where we have written the rational in terms of a triplet of integers, as can always be done [19]. In the equatorial case we know that $\Delta\Phi > 2\pi$ for all eccentric orbits; all relativistic orbits overshoot as the famous precession of the perihelion of Mercury attests. For that reason we have separated out a 1 from the definition of q_Φ in Eq. (39).⁷

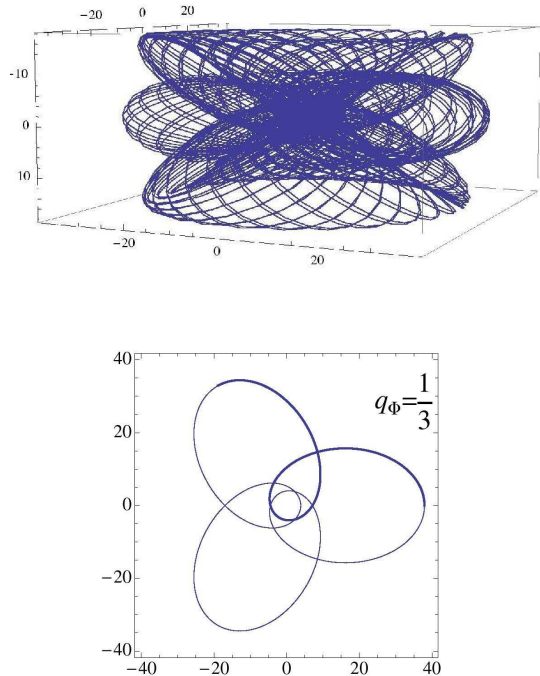


FIG. 5: A $q_\Phi = 1/3$ orbit. The initial conditions are $m_2/m_1 = \frac{1}{4}$, $L = 3.5$, $\theta_{LS} = \frac{\pi}{3}$, $a = 0.9$, and $E = -0.0220582156$. Top: Fully three-dimensional orbit. Bottom: The trajectory is a 3-leaf periodic in the orbital plane. The first radial cycle is in bold.

By analogy with the equatorial Kerr case of Ref. [19], z_Φ counts the number of leaves (or zooms), v_Φ specifies the order in which the leaves are traced out, and w_Φ counts the number of additional full 2π whirls taken between apastron and apastron. To clarify the role of v_Φ , label the leaves sequentially 0 through $z - 1$ starting with the initial apastron. Then v_Φ equals the number of the leaf that the orbit jumps to after the starting apastron. The meaning of the rational is best illustrated with an example. An orbit with $q_\Phi = 1/3$ is shown in Fig. 5. This is a 3-leaf orbit ($z_\Phi = 3$) that moves to the first leaf in the pattern ($v_\Phi = 1$). Since $w_\Phi = 0$, there are no additional whirls from leaf to leaf. In Fig. 6, we show a $q_\Phi = 2/3$ orbit. That is, a 3-leaf orbit ($z_\Phi = 3$) that moves to the second leaf in the pattern ($v_\Phi = 2$). Since $w_\Phi = 0$ there

happens, in this 3PN approximation, it is possible for periodics in the orbital plane to *under-shoot* 2π ; that is, from one apastron to another $\Delta\Phi < 2\pi$ ($q_\Phi < 0$). This never happens with Kerr equatorial orbits and may just be a peculiarity in the approximation, although we won't know for certain until the Kerr non-equatorial case is completed. Also notice that while some orbits may undershoot in the orbital plane, Φ is not the whole story (see the footnote in §IV B) and some of the apparent regression is more than compensated for by Ψ .

⁷ There is an interesting anomaly that has to be mentioned. As it

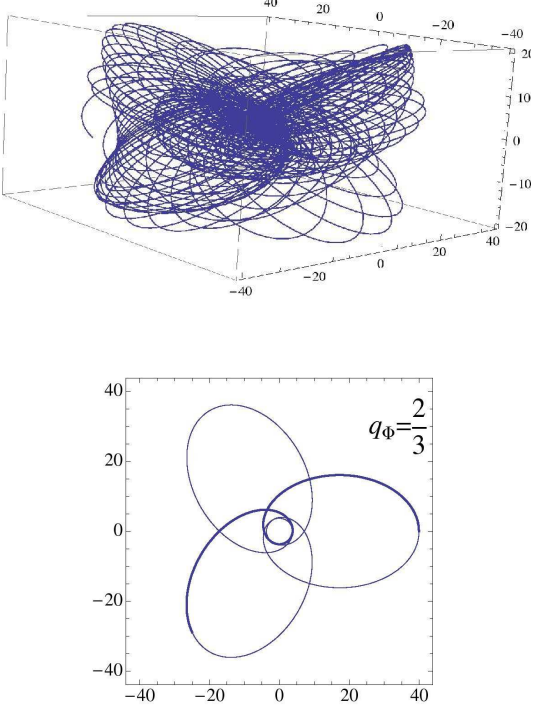


FIG. 6: A $q_\Phi = 2/3$ orbit. The initial conditions are $m_2/m_1 = \frac{1}{4}$, $L = 3.5$, $\theta_{LS} = \frac{\pi}{3}$, $a = 0.9$, and $E = -0.0211669686$. Top: Fully three-dimensional orbit. Bottom: The trajectory is a 3-leaf periodic in the orbital plane that skips a leaf each radial cycle. The first radial cycle is in bold.

are no additional whirls from leaf to leaf. For a z_Φ -leaf orbit, the range of v_Φ for orbits that overshoot, that is precess, is

$$\begin{aligned} 1 \leq v_\Phi \leq z_\Phi - 1, & \quad \text{if } z_\Phi > 1 \\ v_\Phi = 0, & \quad \text{if } z_\Phi = 1 \end{aligned} \quad (40)$$

To avoid degeneracy, we require that z_Φ and v_Φ be relatively prime, or in other words, that $q_\Phi = 2/4$ is the same as $q_\Phi = 1/2$.

The periodic orbits in the orbital plane are a set of measure zero in the space of orbits, just as the rationals are a set of measure zero in the set of the real numbers. However, just as the rationals are dense on \mathbb{R} , the periodics are dense in the space of orbits and so any generic orbit can be arbitrarily well approximated by an orbit that is closed in the orbital plane.

For instance, the orbit of Fig. 7 is very near the 3-leaf orbit and can be interpreted as a precessing 3-leaf orbit. Or we could do better by approximating this orbit as a $q_\Phi = 67/200$, that is, an orbit with 200 leaves that skips to the 67th successive leaf in the pattern with each radial cycle.

By the same token, the randomly selected orbit of Fig. 3 is very nearly a $q_\Phi = 1/5$, that is, a 5-leaf clover, and that of Fig. 4 is very nearly a $q_\Phi = 7/25$ – an orbit with 25

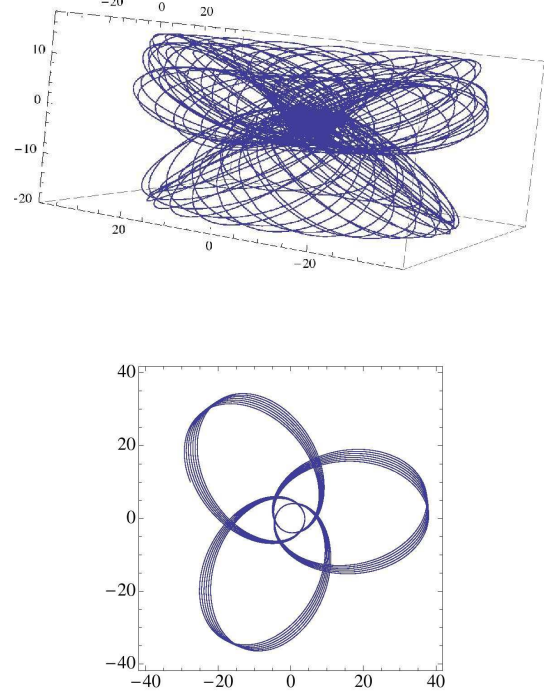


FIG. 7: An orbit for which $q_\Phi = \frac{67}{200}$. The initial conditions are $m_2/m_1 = \frac{1}{4}$, $L = 3.5$, $\theta_{LS} = \frac{\pi}{3}$, $a = 0.9$, and $E = -0.0220323426$. Top: The full three-dimensional orbit. Bottom: The orbit in the orbital plane is a precession of the exact $q_\Phi = 1/3$ orbit.

leaves that skips to the 7th successive leaf in the pattern with each radial cycle.

It is important to notice that although the orbit of Fig. 5 closes in the orbital plane after 3 radial cycles, it does not close in the full three-dimensional space since the orbital plane has not returned to its original location after only 3 radial cycles. A fully closed orbit also has to close in Ψ . Taking the time average of the rate of change $\dot{\Psi}$ over one radial cycle gives the fundamental frequency

$$\omega_\Psi = \frac{2}{T_r} \int_{r_a}^{r_p} \frac{\dot{\Psi}}{\dot{r}} dr = \frac{\Delta\Psi}{T_r} = \omega_r \frac{\Delta\Psi}{2\pi} \quad , \quad (41)$$

so that

$$\frac{\omega_\Psi}{\omega_r} = \frac{\Delta\Psi}{2\pi} \quad . \quad (42)$$

The average precessional frequency may not be rationally related to the radial frequency for a rational q_Φ :

$$\frac{\omega_\Psi}{\omega_r} = \sigma_\Psi \quad , \quad (43)$$

where by σ_Ψ we mean any real number, not just a rational. This time we do not separate out a 1 from the definition of the number. So, σ_Ψ represents the fraction

of 2π swept out as the plane precesses. The orbit of Fig. 5 has a $\sigma_\Psi \approx 0.346\dots$, where we have only listed the first 3 significant figures. Although numerical imprecision of the computer truncates this at a finite number of digits, and therefore effectively approximates σ_Ψ by a rational, it is in principle an irrational. After 3 radial cycles, the orbit has closed in the orbital plane but not in three dimensions. The entire orbital plane has overshoot its initial location by $3\sigma_\Psi - 1 \sim 0.038\dots$. Therefore, even the 3-leaf clover in the orbital plane of Fig. 5 will fill out the surface of the three-dimensional picture.

In fact, from the equations of motion Eqs. (28)-(29), we know that

$$1 + q_\Phi = -\frac{L}{J}\sigma_\Psi + f(E, L) \quad , \quad (44)$$

where $f(E, L)$ is a function of E, L through the dependence of the apastra and periastra's dependence on E, L . This curve for ($m_2/m_1 = 1/4, a = 0.9, \theta_{LS} = \pi/3, L = 3.5$) is shown on the top of Fig. 8. Eq. (44) is interesting for two reasons. It means that σ_Ψ is not generally a rational number when q_Φ is rational. What's even more interesting is that this does not seem to matter. Because q_Φ effectively fixes the value of σ_Ψ for a given L through relation (44), if a generic orbit is well approximated by a periodic in the orbital plane, the precession of its orbital plane is also nearby in the phase space sense.⁸

This point is emphasized on the bottom of Fig. 8, which shows the circle traced out by the precession of the \mathbf{L} vector for the 3-leaf clover in the orbital plane of Fig. 5. The straight line from the origin to the ring indicates the direction of \mathbf{L} after 3 radial cycles have elapsed and the 3-leaf clover has executed one complete period in the orbital plane. The σ_Ψ of this orbit is $\approx 0.346\dots$ so that in 3 radial cycles the orbital plane has just overshoot its initial location. By comparison, the nearby orbit of Fig. 7 has a $\sigma_\Psi \approx 0.348\dots$ and its orbital plane similarly has just barely overshoot its initial location. The orbit of Fig. 7 precesses around the 3-leaf clover of Fig. 5, and its entire orbital plane precesses around \mathbf{J} , sticking close to the precession of the 3-leaf clover's orbital plane. In fact, the precessions of \mathbf{L} are superposed on the bottom of Fig. 8 and the difference between them is imperceptible at the resolution shown. The fact that the precession of \mathbf{L} for these two orbits is effectively indistinguishable confirms that the two orbits are not only near each other in the orbital plane, they are genuinely near each other in 3D as well.

Formally, the above argument ensures that any orbit can be approximated as arbitrarily near an orbit that

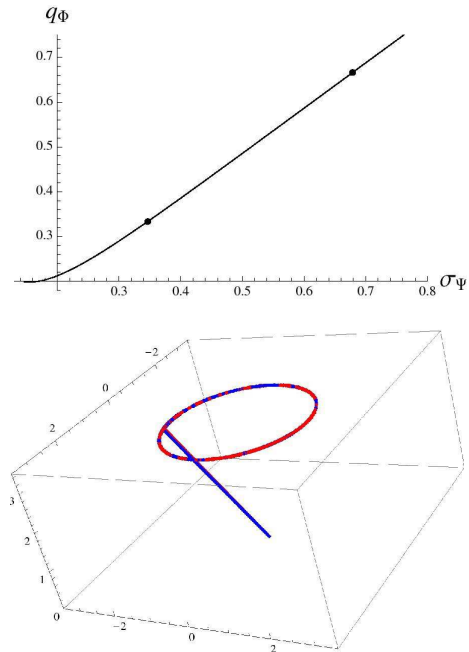


FIG. 8: ($m_2/m_1 = 1/4, a = 0.9, \theta_{LS} = \pi/3, L = 3.5$). Top: q_Φ versus σ_Ψ . The dots mark ($q_\Phi = 1/3, \sigma_\Psi \approx 0.346\dots$) and ($q_\Phi = 2/3, \sigma_\Psi \approx 0.679\dots$). Bottom: The circle traced out by the tip of the vector \mathbf{L} for the orbit of Fig. 5. The straight line represents the \mathbf{L} vector when 3 radial cycles have elapsed and the $q_\Phi = 1/3$ orbit has closed in the orbital plane. The same plot for the precessing 3-leaf clover of Fig. 7 is superposed although the two are so close that they cannot be distinguished in the graph. The fact that they cannot be distinguished confirms that the two orbits are genuinely near each other in 3d as well as in the orbital plane.

is periodic in the orbital plane with the same L . In other words, the orbital periodic spectrum for a given L is dense. If we remove the restriction of comparing orbits of the same L , it follows that the set of orbits periodic in the orbital plane is dense in the entire space. The argument can be sketched as follows. According to Poincaré, the set of orbits that is fully periodic in 3D is dense in the phase space. This set is a subset of the orbital plane periodic set. Therefore, if the subset is dense, the set itself must be dense.

In short, we can understand the entire three-dimensional orbital dynamics through orbits that are closed in the orbital plane and that one rational, not two, is needed for a taxonomy. These conclusions are of course only valid up to 3PN with spin-orbit coupling. In the summary we will discuss the modulation expected by going to higher order in the approximation. In the meantime, we move on to the periodic tables for comparable mass binaries.

⁸ Of course, we can always approximate any irrational, including σ_Ψ by a rational. But then we are describing approximately periodic orbits as opposed to orbits that are formally exactly periodic and there doesn't appear to be any advantage in taking this tack. Hereafter, we will consider σ_Ψ to be generally irrational for any rational q_Φ .

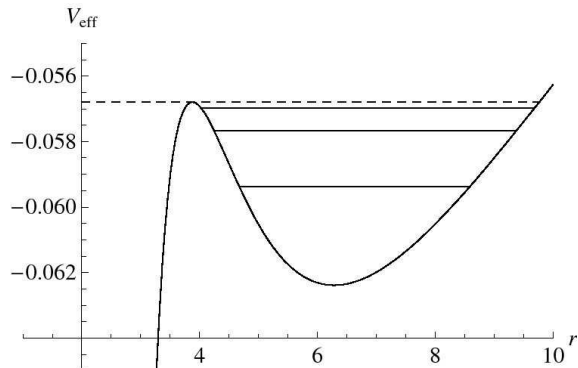


FIG. 9: ($m_2/m_1 = 1/4, a = 0.5, \theta_{LS} = \pi/4$). The pseudo effective-potential as a function of r shows a maximum at the unstable spherical orbit and a minimum at the stable spherical orbit. The homoclinic orbit is indicated with a dashed line. The other lines correspond to, in ascending order, $q_\Phi = \frac{2}{5}, \frac{1}{2}, \frac{2}{3}$. The higher q_Φ orbits quickly stack together near the homoclinic orbit.

IV. PERIODIC TABLES

Since *every* orbit can be approximated as one that is periodic in the orbital plane – just as *every* irrational can be approximated by a rational – we can build a table of orbits for black hole binaries with a given mass ratio, spin, and angle between the spin and the orbital angular momentum ($m_2/m_1, S, L, \theta_{LS}$). Such a periodic table works in analogy to the chemical periodic table as illustrated in Fig. 12. Every entry represents a closed orbit labeled by a rational. The energy and the rationals both increase monotonically from top to bottom and then from left to right. Unlike the chemical periodic table, the black hole periodic tables are infinite since the rationals are infinite and we show only a handful of entries.

When we discuss specific tables, we will always take all entries in a given table to have the same ($m_2/m_1, S, L, \theta_{LS}$). The entries vary only in energy (and therefore in q_Φ). Periodic tables can be constructed for any values of these parameters. However, some ranges give fuller tables in the sense that certain ranges permit more whirliness. To understand the ranges of whirliness requires careful consideration of properties of the spherical orbits. Several results concerning non-equatorial spherical orbits are presented in [29]. Here we summarize the pertinent results for constructing periodic tables with use of a pseudo effective-potential picture.

A sensible condition for an effective potential formulation is that the Hamiltonian depend only on r and constants. Generally, the Hamiltonian of Eqs. (2)-(5) does not admit a simple effective potential formulation since it is a complicated function of \mathbf{p}^2 . We have already argued that $H(r, \mathbf{p}, \mathbf{S})$ can be written as a radial Hamiltonian $H(r, P_r)$, yet it remains a complicated function of P_r . However, if we only consider

$$V_{\text{eff}} = H(P_r = 0) \quad , \quad (45)$$

then we have a good representation of the effective potential *at the turning points*. We cannot misuse the V_{eff} by trying to interpret motion away from the turning points, but it gives a perfectly valid description of the behavior at apelia and periastra as well as on spherical orbits. Hereafter we’ll shorthand the term “pseudo effective-potential” by “effective potential”. An effective potential for comparable mass binaries is shown in Fig. 9.

Evident is the lowest energy orbit at the stable spherical orbit. The highest energy non-plunging orbit is the unstable spherical orbit. We are interested in energetically bound orbits here, i.e. orbits with $E \leq 0$. If the unstable spherical orbit has energy $E < 0$, then the spectrum of periodic orbits densely fills the energy range between the stable and unstable spherical orbit. If instead the unstable spherical orbit has energy $E > 0$, then the spectrum of periodic orbits densely fills the energy range between the stable spherical orbit and the marginally bound orbit at $E = 0$. The energy levels of a few periodic orbits are indicated by solid lines in Fig. 9.

Since q_Φ is monotonic with energy, the entries in the periodic table are bounded:

$$q_{\min} \leq q_\Phi \leq q_{\max} \quad . \quad (46)$$

The value of q_{\min} is the q_Φ of the stable spherical orbit and q_{\max} is set by the q_Φ of the maximum energy bound orbit.

The value of q_{\max} depends on the largest energy orbit allowed for that L . When an unstable spherical orbit exists there is always an orbit with the same E and L at a large radius. The maximum of V_{eff} in Fig. 9 marks the unstable spherical orbit. Drawing a line of constant energy across the effective potential locates the apastron of the orbit with the same E and L as the unstable spherical trajectory. When released from apastron, this orbit whirls an infinite number of times as it approaches the unstable spherical orbit and is formally a homoclinic orbit; that is, it approaches the same invariant set in the infinite future and the infinite past. Although not strictly periodic – the homoclinic orbit never returns to apastron – it can be considered the infinite winding limit of the 1-leaf periodic orbits [19]. As such it is the $w_\Phi = \infty$ limit and we assign homoclinic orbits a $q_\Phi = \infty$. Consequently, if the range of parameters has a bound unstable spherical orbit, then it has a ($q_\Phi = \infty$) homoclinic orbit and the associated periodic tables will exhibit much whirliness.

Since, for a given L , the stable spherical orbits bound the allowed energy range from below, they also bound the value of q_Φ from below. One might presume that $q_{\min} = 0$ but, importantly, this is not the case. To see this notice that a spherical orbit obviously does not have a radial cycle. The q_{\min} set by the stable spherical orbit can instead be thought of as the value of q_Φ for a nearby eccentric orbit in the limit that the eccentricity vanishes:

$$q_{\min} \rightarrow \lim_{e \rightarrow 0} \frac{\omega_\Phi}{\omega_r} - 1 \quad . \quad (47)$$

This allows us to derive the q_{min} from a stability analysis since the limit of zero eccentricity is effectively the limit of constant radius, which implies $\dot{\Phi}|_{r_s}$ is constant and that $\omega_r = i\lambda_r$ is given by a small perturbation around the stable spherical orbit. We then have, just as we found in Ref. [19] that⁹

$$q_{min}(r_s) = \frac{\dot{\Phi}|_{r_s}}{|\lambda_r|} - 1 \quad . \quad (48)$$

We choose for the sake of illustration to consider tables capable of probing high whirliness. For this reason we stay within the range set by the last stable spherical orbit (LSSO) and the homoclinic orbit $L_{LSSO} < L < L_{homoclinic}$. Of course, the drawback is that we are pushing the PN expansion to the breaking point. Although these inner strong-field orbits probe beyond the confidence of the 3PN approximation, the general method of constructing periodic tables in a full relativistic treatment is robust, as proven by the Kerr demonstration of Ref. [19].

A. Periodic Tables in the Orbital Plane

The purpose of the Post-Newtonian expansion is of course to approximate the behavior of comparable mass binaries. A periodic table for a binary with $m_2/m_1 = 1/4$ is shown in Fig. 10. The heavier black hole has a spin amplitude of $a = 1/2$ and the angle is $\hat{\mathbf{L}} \cdot \hat{\mathbf{S}} = \cos(\pi/4)$. The orbits do not lie in a plane and are fully three-dimensional, like those of Figs. 3 and 4. Each entry is an orbit that is periodic in the orbital plane, although not necessarily fully periodic. The energy and the rational of each entry increase from top to bottom and from left to right.

Notice that the first two entries are blank before the appearance of the 2-leaf clover in entry 3. These are blank because, for this $(m_2/m_1, a, S, L, \theta_{LS})$, the $q_\Phi = 0$ and $q_\Phi = 1/3$ orbits simply do not exist since q_{min} is just above $1/3$ (and $q_{max} = \infty$). We saw this before in the Kerr system [19]. The implication is important. *All* eccentric orbits – for this range of parameters – show zoom-whirl behavior. None of them look like the slight precession of the perihelion of Mercury.

⁹ Although most orbits precess in the orbital plane, Eq. (48) actually allows for regression when $\frac{\dot{\Phi}|_{r_s}}{|\lambda_r|} < 1$. When the orbital plane and the equatorial plane align $(\mathbf{S} \times \mathbf{L}) = 0$, then regression seems intuitively obvious. It only means that Φ is not the whole story of the motion of $\hat{\mathbf{n}}$ and we must also add in Ψ to see that the actual orbit precesses in the equatorial plane, as we will do explicitly by moving to the equatorial basis in §IV B. We did however also see regression out of the equatorial plane and it is difficult to say whether it is a flaw in the PN approximation or if it will survive a full relativistic treatment.

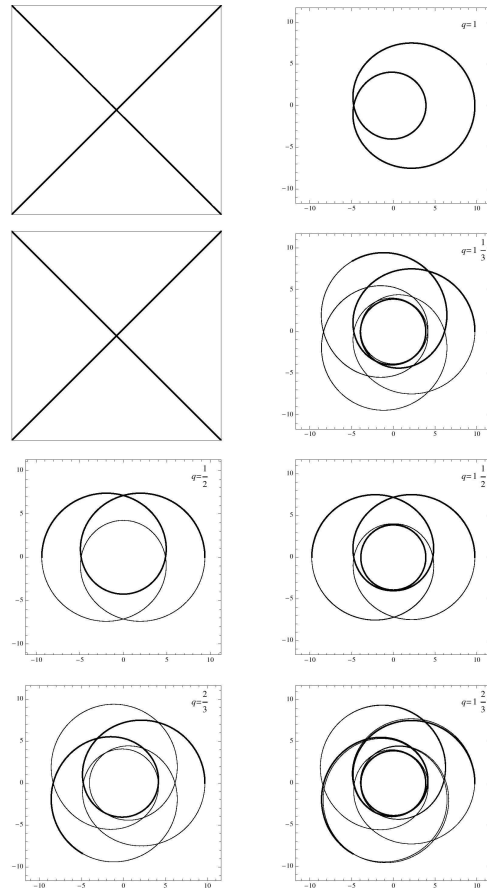


FIG. 10: A non-equatorial periodic table for which the heavier black hole spins with amplitude $a = \frac{1}{2}$, the mass ratio is $m_2/m_1 = \frac{1}{4}$, $L = 3.2$ and $\theta_{LS} = \frac{\pi}{4}$. All valid entries up to $z_\Phi = 3$ are shown. The final entry begins to show a departure from true periodicity as a result of numerical error. The high numerical precision required to keep the simulated orbit near a perfectly periodic one is a reflection of the tight stacking of high q_Φ orbits near the top of the potential in Fig. 9.

Every orbit in this system can be arbitrarily well-approximated by an entry in the table, because the precessional motion of the entire plane is also effectively fixed by the rational q_Φ as the plot of Fig. 11 shows. If σ_Ψ could be chosen independently of q_Φ for a given L , our conclusion would not follow. However, q_Φ versus σ_Ψ lies on a one-dimensional curve. Once q_Φ is known, σ_Ψ can be read off. Physically this means that an orbit that is very near a $q_\Phi = 1/2$ will precess around the 2-leaf clover in the orbital plane and that the precession of the entire orbital plane will be very close to the precession of the true 2-leaf clover's orbital plane.

B. Periodic Tables in the Equatorial Plane

Some binary parameters will automatically restrict motion to the *equatorial* plane and these require special discussion. For instance, if neither black hole spins

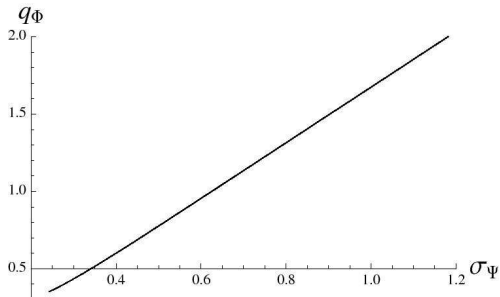


FIG. 11: q_Φ versus σ_Ψ for the table in Fig. 10.

then the system is spherically symmetric and all orbits are confined to a plane: the orbital plane *is* the equatorial plane. Similarly, if one of the black holes spins but the spin is aligned with the angular momentum or anti-aligned, then the motion will again be restricted to the equatorial plane. We summarize these three cases as $\mathbf{S} \times \mathbf{L} = 0$ scenarios.

When $\mathbf{S} \times \mathbf{L} = 0$, our orbital basis $(\hat{\mathbf{n}}, \hat{\Phi}, \hat{\Psi})$ is not defined and must be replaced with the usual planar basis $(\hat{\mathbf{n}}, \hat{\varphi})$, where φ is the usual angle measured¹⁰ between $\hat{\mathbf{n}}$ and $\hat{\mathbf{i}}$. The equation of motion for φ is simply

$$\dot{\varphi} = \dot{\Phi} + \dot{\Psi} \quad . \quad (49)$$

The q we must use for the equatorial plane of the non-spinning system is then the same as the one we used in Ref. [19]

$$\frac{\omega_\varphi}{\omega_r} = 1 + q \quad . \quad (50)$$

Each entry is specified by this one rational which represents the ratio of the time averaged orbital angular frequency in the equatorial plane to the radial frequency, just as in the Kerr case of Ref. [19]. The rational can be read off the topology of the orbit as $q = w + v/z$; that is, the number of whirls, the number of leaves and the order in which the leaves are laid out fix q .

The table of Fig. 12 reflects a non-spinning black hole system with an extreme mass ratio of $m_2/m_1 = 10^{-6}$. The first 3 entries are blank since q_{min} is just below $1/2$. Although we only show entries up to $z_\Phi = 4$ for $w_\Phi \leq 2$, for these parameters $q_{max} = \infty$.¹² Although we defer a detailed comparison between the 3PN spin-orbit system of this paper and the Kerr system, we point out the intriguing possibility that periodic tables could be used to further test the accuracy of the Post-Newtonian expansion [21].

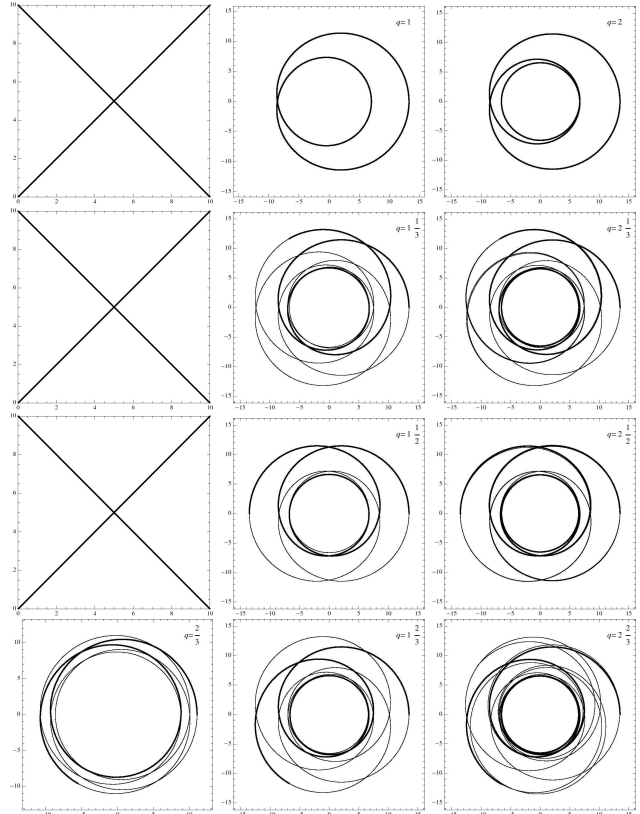


FIG. 12: A periodic table for orbits in a non-spinning system $a = 0$, extreme-mass-ratio system, $\frac{m_2}{m_1} = 10^{-6}$. The angular momentum is $L = 3.9$. Since $a = 0$ all orbits lie in the equatorial plane. Periodic tables such as this one could be used to expand on comparisons with the full relativistic system. All valid entries up to $z_\Phi = 4$ are shown. As before, the final entry begins to show a departure from true periodicity as a result of numerical error.

V. CONCLUSIONS

To recap in bullet format, for comparable mass binaries with one spinning black hole and one non-spinning black hole as approximated by the 3PN Hamiltonian plus spin-orbit coupling, our main results are:

1. Simplified Equations of Motion in an Orbital Basis

From which we find

- constant aphelia and perihelia for non-equatorial eccentric orbits, and
- three fundamental frequencies that depend only on radius.

and

2. Taxonomy of Fully Three-Dimensional Orbits

For which we find

¹⁰ If we were epsilon out of the equatorial plane, we would see regression in the orbital plane because much of the motion is taken through Ψ . Intuitively then, those instance of regression that are just barely out of the equatorial plane are not that surprising.

- there exists a spectrum of closed orbits in the orbital plane corresponding to a subset of the rationals;
- one rational, not two is required for an orbital plane taxonomy of constant angular momentum slices;
- *all* orbits can be approximated as near an orbit that is perfectly closed in the orbital plane; and
- zoom-whirl behavior is ubiquitous in comparable mass binary dynamics and entirely quantifiable through the spectrum of rationals.

The first discovery we made in Ref. [19] with our periodic taxonomy for equatorial Kerr orbits is that precessing elliptical orbits such as Mercury’s are excluded in the strong-field Kerr regime – just as Keplerian ellipses are excluded in any relativistic regime. Instead, at close separations, *all* equatorial Kerr eccentric orbits trace out precessions of patterns best described as multi-leaf clovers, whirling around the central black hole before zooming out quasi-elliptically [47, 48]. In this paper we have found that this same conclusion applies in the strong-field regime of our comparable mass black hole binaries, even out of the equatorial plane. Our periodic tables in the orbital plane show zoom-whirl behavior as the norm in the strong-field regime and not as the exception.

The further importance of the orbital dynamics lies in its direct imprint in the gravitational waveform [49, 50]. The waveform will necessarily reflect the features above. For instance, an equatorial circular orbit (neglecting radiation reaction) is described by essentially one frequency. By contrast, *all other orbits* in the strong-field regime generate highly modulated waveforms naturally described by harmonics of the 3 orbital basis frequencies, which in turn directly correspond to the natural frequencies of a nearby periodic orbit.

Naturally, we should ask about the astrophysical likeliness of detecting any such orbits with either the LIGO or LISA observatories. Although estimates vary [51], stellar mass black hole pairs are currently the favored source for advanced ground-based detectors and intermediate mass black hole pairs are considered an important objective for space-based LISA science. It is challenging to definitively assess the spins and eccentricities of black hole/black hole binaries given the absence of observational constraints [52]. Still, one can guess that long-lived stellar binaries that might collapse to a pair of bound black holes would circularized by the time the pair enters the strong-field due to angular momentum lost in the form of gravitational radiation.¹¹ By contrast, for shorter-lived black hole binaries formed in globular clusters, the astrophysical likeliness of eccentric orbits sliding in the LIGO bandwidth is assessed to be $\gtrsim 30\%$ for eccentricities > 0.1 in Ref. [31]. All such binaries would necessarily transit near the periodic set on inspiral. Even

if the inspiral happens too quickly to witness multiple executions near a low-leaf clover, the orbit can still be sewn together as a skip from a piece of one periodic to a piece of another. Finally, the spins and eccentricities of intermediate black hole binaries detectable by LISA are most difficult to predict although we should expect them to spend a more generous allotment of windings on eccentric orbits in the strong-field.

Before closing, we have to mention the effects of spin-spin coupling on the orbital basis picture. The spin-spin correction introduces additional precessions of the spin and this destroys the constancy of the angle between $\mathbf{S}\cdot\mathbf{L}$ and generally introduces explicit angular dependence in the equations of motion. Interpreted as a small perturbation to the system here, the spin-spin couplings cause additional wobbling of the precessional motion.

When both objects spin, the impact of spin-spin coupling can be particularly destructive. It is by now well documented that two spinning black holes in comparable mass binaries exhibit chaotic motion in the conservative system [27, 38, 39, 40, 41, 42, 43, 44]. There are not enough constants of the motion to ensure regular behavior. Even the restricted spin-orbit scenario of this paper is clearly vulnerable to chaos even perturbed as it admits a homoclinic orbit. Under perturbation, homoclinic orbits tend to disrupt into a homoclinic tangle, an infinite intersection of stable and unstable manifolds. At root, chaos emerges as periodic orbits proliferate in a bounded region of space. Our clean taxonomy of periodic orbits corresponding to a simple set of rationals would give way to a glut of periodic orbits corresponding to some fractal set, as in systems with a strange repeller – the Hamiltonian analog to the strange attractor. The complex motion may be damped by energy and angular momentum losses to gravitational waves but, at the least, chaos signals the breakdown of the simple set of periodic orbits. The onset of chaos can be directly identified with the spin-spin couplings, and we leave this task to a forthcoming companion paper [29].

Acknowledgments

We are especially thankful to Gabe Perez-Giz for his valuable and generous contributions to this work and to Jamie Rollins for his careful reading of the manuscript. We also thank Szabi Marka for important discussions. JL and BG gratefully acknowledge the support of a Columbia University ISE grant. This material is based in part upon work supported under a National Science Foundation Graduate Research Fellowship.

¹¹ However, when spin-spin coupling is included, there are no circular or even spherical orbits [29].

APPENDIX A: PROJECTION OF THE EQUATIONS OF MOTION ONTO THE NON-ORTHOGONAL ORBITAL BASIS

1. Projection onto Orbital Basis

By projecting the equations of motion onto the orbital basis $(\hat{\mathbf{n}}, \hat{\Phi}, \hat{\Psi})$, we show here that the equations of motion depend only on the radius.

The four equations of motion in the orbital plane are obtained by projecting Hamilton's equations onto the basis vectors, as is done in celestial mechanics. For now, consider only the projections onto the orbital basis vectors to generate the four equations,

$$\begin{aligned} \dot{\mathbf{r}} \cdot \hat{\mathbf{n}} &= \frac{\partial H}{\partial \mathbf{p}} \cdot \hat{\mathbf{n}} \\ \dot{\mathbf{r}} \cdot \hat{\Phi} &= \frac{\partial H}{\partial \mathbf{p}} \cdot \hat{\Phi} \\ \dot{\mathbf{p}} \cdot \hat{\mathbf{n}} &= -\frac{\partial H}{\partial \mathbf{r}} \cdot \hat{\mathbf{n}} \\ \dot{\mathbf{p}} \cdot \hat{\Phi} &= -\frac{\partial H}{\partial \mathbf{r}} \cdot \hat{\Phi} \end{aligned} \quad (\text{A1})$$

To break down the LHS and RHS of the above projections it will be useful to write

$$\mathbf{p} = (\mathbf{p} \cdot \hat{\mathbf{n}})\hat{\mathbf{n}} + (\hat{\mathbf{n}} \times \mathbf{p}) \times \hat{\mathbf{n}} \quad (\text{A2})$$

$$= P_r \hat{\mathbf{n}} + \frac{\mathbf{L}}{r} \times \hat{\mathbf{n}} \quad (\text{A3})$$

$$= P_r \hat{\mathbf{n}} + \frac{L}{r} \hat{\Phi} \quad (\text{A4})$$

where the component $p_r = P_r$ and by capitol P 's we mean canonical momenta versus small case, which will mean components. To break down the LHS involves

$$\begin{aligned} \dot{\mathbf{r}} &= \dot{r}\hat{\mathbf{n}} + r\dot{\hat{\mathbf{n}}} \\ \dot{\mathbf{p}} &= \dot{P}_r \hat{\mathbf{n}} + P_r \dot{\hat{\mathbf{n}}} - \frac{L}{r^2} \dot{r} \hat{\Phi} + \frac{L}{r} \dot{\hat{\Phi}} \end{aligned} \quad (\text{A5})$$

So, we will need $\dot{\hat{\mathbf{n}}}$ and $\dot{\hat{\Phi}}$, which are most directly obtained by expanding $(\hat{\mathbf{n}}, \hat{\Phi})$ in the $(\hat{\mathbf{X}}, \hat{\mathbf{Y}})$ basis and then expanding $(\hat{\mathbf{X}}, \hat{\mathbf{Y}})$ in the Cartesian basis. So, we will need

$$\begin{aligned} \hat{\mathbf{n}} &= \cos \Phi \hat{\mathbf{X}} + \sin \Phi \hat{\mathbf{Y}} \\ \hat{\Phi} &= -\sin \Phi \hat{\mathbf{X}} + \cos \Phi \hat{\mathbf{Y}} \\ \hat{\mathbf{X}} &= \cos \Psi \hat{\mathbf{i}} + \sin \Psi \hat{\mathbf{j}} \\ \hat{\mathbf{Y}} &= \sin \theta_Y (-\sin \Psi \hat{\mathbf{i}} + \cos \Psi \hat{\mathbf{j}}) + \cos \theta_Y \hat{\mathbf{k}} \\ \hat{\Psi} &= -\sin \Psi \hat{\mathbf{i}} + \cos \Psi \hat{\mathbf{j}} \end{aligned} \quad (\text{A6})$$

Using

$$\dot{\hat{\mathbf{X}}} = \dot{\Psi} \hat{\Psi} = \Omega_L \hat{\Psi} \quad (\text{A7})$$

$$\dot{\hat{\Psi}} = -\dot{\Psi} \hat{\mathbf{X}} = -\Omega_L \hat{\mathbf{X}} \quad (\text{A8})$$

$$\dot{\hat{\mathbf{Y}}} = \sin \theta_Y \dot{\hat{\Psi}} = -\sin \theta_Y \Omega_L \hat{\mathbf{X}} \quad (\text{A9})$$

where $\dot{\Psi} = \Omega_L = \delta_1 J / r^3$ from Eq. (26) so that we have $\dot{\hat{\mathbf{n}}}$:

$$\begin{aligned} \dot{\hat{\mathbf{n}}} &= \dot{\hat{\Phi}} \hat{\Phi} + \cos \Phi \dot{\hat{\mathbf{X}}} + \sin \Phi \dot{\hat{\mathbf{Y}}} \\ &= \dot{\hat{\Phi}} \hat{\Phi} + \Omega_L \left(\cos \Phi \hat{\Psi} - \sin \Phi \sin \theta_Y \hat{\mathbf{X}} \right) \\ &= \dot{\hat{\Phi}} \hat{\Phi} + \frac{\Omega_L}{\sin \theta_Y} \left(\cos \Phi \hat{\mathbf{Y}} - \cos \Phi \cos \theta_Y \hat{\mathbf{k}} - \sin \Phi \sin^2 \theta_Y \hat{\mathbf{X}} \right) \end{aligned} \quad (\text{A10})$$

To take the projection of Eqs. (A1) we will also need

$$\begin{aligned} \hat{\mathbf{n}} \cdot \hat{\mathbf{X}} &= \cos \Phi & \hat{\Phi} \cdot \hat{\mathbf{X}} &= -\sin \Phi \\ \hat{\mathbf{n}} \cdot \hat{\mathbf{Y}} &= \sin \Phi & \hat{\Phi} \cdot \hat{\mathbf{Y}} &= \cos \Phi \\ \hat{\mathbf{n}} \cdot \hat{\mathbf{k}} &= \sin \Phi \cos \theta_Y & \hat{\Phi} \cdot \hat{\mathbf{k}} &= \cos \Phi \cos \theta_Y \end{aligned} \quad (\text{A11})$$

In the last step we use

$$\hat{\mathbf{k}} \cdot \hat{\mathbf{n}} = \hat{\mathbf{J}} \cdot (\cos \Phi \hat{\mathbf{X}} + \sin \Phi \hat{\mathbf{Y}}) = \sin \Phi \hat{\mathbf{J}} \cdot \hat{\mathbf{Y}} \quad (\text{A12})$$

since $\hat{\mathbf{X}}$ lies in the equatorial plane, it is by definition perpendicular to $\hat{\mathbf{J}} = \hat{\mathbf{k}}$. From all of the above relations we obtain for use in the projections

$$\dot{\hat{\mathbf{n}}} \cdot \hat{\mathbf{n}} = 0 \quad (\text{A13})$$

$$\dot{\hat{\mathbf{n}}} \cdot \hat{\Phi} = \dot{\hat{\Phi}} + \Omega_L \sin \theta_Y = \dot{\hat{\Phi}} + \Omega_L \cos \theta_L \quad (\text{A14})$$

Now for $\dot{\hat{\Phi}}$. Taking the derivative of $\hat{\Phi}$ as expressed in Eq. (A6) we have

$$\begin{aligned}
\dot{\hat{\Phi}} &= -\dot{\Phi}\hat{\mathbf{n}} - \sin\Phi\dot{\hat{\mathbf{X}}} + \cos\Phi\dot{\hat{\mathbf{Y}}} \\
&= -\dot{\Phi}\hat{\mathbf{n}} + \Omega_L \left(-\sin\Phi\hat{\Psi} - \cos\Phi\sin\theta_Y\hat{\mathbf{X}} \right) \\
&= -\dot{\Phi}\hat{\mathbf{n}} + \frac{\Omega_L}{\sin\theta_Y} \left(-\sin\Phi\hat{\mathbf{Y}} + \sin\Phi\cos\theta_Y\hat{\mathbf{k}} - \cos\Phi\sin^2\theta_Y\hat{\mathbf{X}} \right)
\end{aligned} \tag{A15}$$

and using Eqs. (A11), we have for use in the projections of Eqs. (A1),

$$\begin{aligned}
\dot{\hat{\Phi}} \cdot \hat{\mathbf{n}} &= -\left(\dot{\Phi} + \Omega_L \sin\theta_Y\right) = -\left(\dot{\Phi} + \Omega_L \cos\theta_L\right) \\
\dot{\hat{\Phi}} \cdot \hat{\Phi} &= 0
\end{aligned} \tag{A16}$$

Now we can derive the equations of motion in the (r, Φ, Ψ) coordinates. From the equations we constructed in section §II C,

$$\begin{aligned}
\dot{\mathbf{r}} &= A\mathbf{p} + B\hat{\mathbf{n}} + \delta_1 \frac{\mathbf{S} \times \mathbf{r}}{r^3} \\
\dot{\mathbf{p}} &= C\mathbf{p} + D\hat{\mathbf{n}} + \delta_1 \frac{\mathbf{S} \times \mathbf{p}}{r^3} + 3\delta_1 \frac{\mathbf{L} \cdot \mathbf{S}}{r^4} \hat{\mathbf{n}}
\end{aligned} \tag{A17}$$

and the projections (Eqs. (A1)), with all of the the above vector relations we have the radial equation,

$$\dot{\mathbf{r}} \cdot \hat{\mathbf{n}} = \dot{r} = AP_r + B \tag{A18}$$

The Φ equation is found from

$$\dot{\mathbf{r}} \cdot \hat{\Phi} = \frac{\partial H}{\partial \mathbf{p}} \cdot \hat{\Phi} \tag{A19}$$

$$r \left(\dot{\Phi} + \Omega_L \cos\theta_L \right) = A \frac{L}{r} + \delta_1 \frac{(\mathbf{S} \times \mathbf{r}) \cdot \hat{\Phi}}{r^3} \tag{A20}$$

Look at

$$(\mathbf{S} \times \mathbf{r}) \cdot \hat{\Phi} = r (\mathbf{S} \cdot \hat{\mathbf{L}}) \tag{A21}$$

The Φ equation is then

$$\dot{\Phi} = A \frac{L}{r^2} + \Omega_L \left(-\cos\theta_L + \frac{\mathbf{S} \cdot \hat{\mathbf{L}}}{J} \right) \tag{A22}$$

where $\hat{\mathbf{S}} \cdot \hat{\mathbf{L}}$ is constant. Another helpful relation is

$$\frac{\mathbf{S} \cdot \hat{\mathbf{L}}}{J} = \hat{\mathbf{J}} \cdot \hat{\mathbf{L}} - \frac{L}{J} = \cos\theta_L - \frac{L}{J} \tag{A23}$$

allowing us to write the Φ equation in its final form,

$$\dot{\Phi} = A \frac{L}{r^2} - \Omega_L \frac{L}{J} \tag{A24}$$

The two conjugate momenta equations are next. We start with P_r :

$$\begin{aligned}
\dot{\mathbf{p}} \cdot \hat{\mathbf{n}} &= \dot{P}_r - \frac{L}{r} (\dot{\Phi} + \Omega_L \cos\theta_L) \\
&= CP_r + D + 2\Omega_L \frac{\mathbf{S} \cdot \mathbf{L}}{Jr}
\end{aligned} \tag{A25}$$

where we have used that

$$(\mathbf{p} \times \mathbf{S}) \cdot \hat{\mathbf{n}} = \frac{\mathbf{S} \cdot \mathbf{L}}{r} \tag{A26}$$

Notice if we use Eq. (A22), we have

$$\dot{P}_r = A \frac{L^2}{r^3} + CP_r + D + 3\Omega_L \frac{\mathbf{S} \cdot \mathbf{L}}{Jr}$$

and last

$$\begin{aligned}
\dot{\mathbf{p}} \cdot \hat{\Phi} &= P_r (\dot{\Phi} + \Omega_L \cos\theta_L) - \frac{L}{r^2} \dot{r} \\
&= C \frac{L}{r} + \Omega_L \frac{P_r \mathbf{S} \cdot \hat{\mathbf{L}}}{J}
\end{aligned} \tag{A27}$$

where we have used that

$$(\mathbf{p} \times \mathbf{S}) \cdot \hat{\Phi} = \mathbf{S} \cdot (\hat{\Phi} \times \mathbf{p}) = -P_r \mathbf{S} \cdot \hat{\mathbf{L}} \tag{A28}$$

Notice if we use Eq. (A22), we have a cancellation and

$$(AP_r - \dot{r}) \frac{L}{r^2} = -B \frac{L}{r} = C \frac{L}{r}$$

which confirms a true statement but does not provide any new equation of motion since we implicitly used $\dot{L} = 0$. We will show in the next subsection that the canonical momentum $P_\Phi = L$ and so the last equation of motion corresponds to $\dot{P}_\Phi = 0$. All four equations in the orbital basis are compiled in the boxed Eqs. (28).

2. Conjugate Momenta for Φ and Ψ

We can show that the momentum conjugate to Φ is $P_\Phi = L$ and the momentum conjugate to Ψ is $P_\Psi = L_z = L \cos\theta_L$. So the equations of motion (Φ, P_Φ) and (Ψ, P_Ψ) should be derivable from

$$\begin{aligned}
\dot{\Phi} &= \frac{\partial H}{\partial P_\Phi}, & \dot{P}_\Phi &= 0 \\
\dot{\Psi} &= \frac{\partial H}{\partial P_\Psi}, & \dot{P}_\Psi &= 0
\end{aligned} \tag{A29}$$

This is far more elaborate than one might guess and so we spend this last subsection verifying that L and L_z are the conjugate momenta and that the equations of motion derived according to (A29) are in fact the same as those of Eqs. (28).

We begin by showing that $P_\Phi = L$ and $P_\Psi = L_z$ are consistent with our equations before we explicitly rederive the equations of motion using (A29). Bear in mind that the variables (r, Φ, Ψ) and their conjugate momenta must be linearly independent and so $\partial X^i / \partial X^j = \delta_j^i$ where $X = (r, P_r, \Phi, P_\Phi, \Psi, P_\Psi)$. We also need to be careful to rewrite everything in terms of (r, Φ, Ψ) and the conjugate momenta (P_r, L, L_z) . Particularly, we will need to take the derivative of terms like $\cos \theta_L = P_\Psi / P_\Phi = L_z / L$. From Eqs. (A29) we have that

$$\begin{aligned} \dot{\Phi} &= \frac{\partial H}{\partial P_\Phi} = \frac{\partial H}{\partial \mathbf{p}} \cdot \frac{\partial \mathbf{p}}{\partial P_\Phi} + \frac{\partial H}{\partial \mathbf{r}} \cdot \frac{\partial \mathbf{r}}{\partial P_\Phi} \\ &= \dot{\mathbf{r}} \cdot \frac{\partial \mathbf{p}}{\partial L} - \dot{\mathbf{p}} \frac{\partial \mathbf{r}}{\partial L} \end{aligned} \quad (\text{A30})$$

Now

$$\begin{aligned} \dot{\mathbf{r}} &= \dot{r} \hat{\mathbf{n}} + r \dot{\hat{\mathbf{n}}} \\ \dot{\mathbf{p}} &= \dot{P}_r \hat{\mathbf{n}} + P_r \dot{\hat{\mathbf{n}}} - \frac{L \dot{r}}{r^2} \hat{\Phi} + \frac{L}{r} \dot{\hat{\Phi}} \end{aligned} \quad (\text{A31})$$

and

$$\begin{aligned} \frac{\partial \mathbf{p}}{\partial L} &= P_r \frac{\partial \hat{\mathbf{n}}}{\partial L} + \frac{L}{r} \frac{\partial \hat{\Phi}}{\partial L} + \frac{1}{r} \hat{\Phi} \\ \frac{\partial \mathbf{r}}{\partial L} &= r \frac{\partial \hat{\mathbf{n}}}{\partial L} \end{aligned} \quad (\text{A32})$$

The unit vectors $\hat{\mathbf{n}}$ and $\hat{\Phi}$ depend on L and L_z through $\cos \theta_L = L_z / L$. Using Eq. (A6) and replacing $\sin \theta_Y$ with $\cos \theta_L$ etc. we have

$$\begin{aligned} \frac{\partial \hat{\mathbf{n}}}{\partial L} &= \sin \Phi \frac{\partial \hat{\mathbf{Y}}}{\partial L} = -\sin \Phi \frac{\cos \theta_L}{L} \left(\hat{\Psi} - \cot \theta_L \hat{\mathbf{k}} \right) \\ \frac{\partial \hat{\Phi}}{\partial L} &= \cos \Phi \frac{\partial \hat{\mathbf{Y}}}{\partial L} = -\cos \Phi \frac{\cos \theta_L}{L} \left(\hat{\Psi} - \cot \theta_L \hat{\mathbf{k}} \right) \end{aligned} \quad (\text{A33})$$

Using Eq. (A10) for $\dot{\hat{\mathbf{n}}}$ and Eq. (A14) for $\dot{\hat{\Phi}}$, Eq. (A30) becomes

$$\dot{\Phi} = \dot{\Phi} + \dot{\Psi} \cos \theta_L + \frac{\cos \theta_L}{L} \left(\cot \theta_L \hat{\mathbf{k}} - \hat{\Psi} \right) \cdot \left[\left(P_r \sin \Phi + \frac{L}{r} \cos \Phi \right) \left(\dot{r} \hat{\mathbf{n}} + r \dot{\hat{\mathbf{n}}} \right) - r \sin \Phi \left(\dot{P}_r \hat{\mathbf{n}} + P_r \dot{\hat{\mathbf{n}}} - \frac{L \dot{r}}{r^2} \hat{\Phi} + \frac{L}{r} \dot{\hat{\Phi}} \right) \right]$$

Taking the dot products, there are some fortunate cancellations and overall we find

$$\dot{\Phi} = \dot{\Phi} + \dot{\Psi} \cos \theta_L - \dot{\Psi} \cos \theta_L = \dot{\Phi} \quad (\text{A34})$$

As claimed, $P_\Phi = L$ is consistent. The same procedure for Ψ with $P_\Psi = L_z$ yields a similarly consistent equality.

Now, to derive the equations of motion directly from

$$\dot{\Phi} = \frac{\partial H}{\partial L} = \frac{\partial H_{PN}}{\partial L} + \frac{\partial H_{SO}}{\partial L} \quad (\text{A35})$$

is tedious but doable. The PN piece is straightforward if one first writes everything in terms of canonical variables; i.e., $(\hat{\mathbf{n}} \cdot \mathbf{p}) = P_r$ and $\mathbf{p}^2 = P_r^2 + P_\Phi^2 / r^2 = P_r^2 + L^2 / r^2$, then

$$\frac{\partial H_{PN}}{\partial L} = A \frac{L}{r^2} \quad (\text{A36})$$

The partial of the spin orbit piece is

$$\begin{aligned} \frac{\partial H_{SO}}{\partial L} &= \frac{\delta_1 \mathbf{S}}{r^3} \cdot \frac{\partial (\mathbf{r} \times \mathbf{p})}{\partial L} \\ &= \frac{\delta_1 \mathbf{S}}{r^3} \cdot \left[r \frac{\partial \hat{\mathbf{n}}}{\partial L} \times \mathbf{p} + \mathbf{r} \times \frac{\partial \mathbf{p}}{\partial L} \right] \\ &= \frac{\delta_1 \mathbf{S}}{r^3} \cdot \left[r \frac{\partial \hat{\mathbf{n}}}{\partial L} \times \mathbf{p} + \mathbf{r} \times \left(P_r \frac{\partial \hat{\mathbf{n}}}{\partial L} + \frac{L}{r} \frac{\partial \hat{\Phi}}{\partial L} + \frac{\hat{\Phi}}{r} \right) \right] \end{aligned}$$

Replace $P_r \hat{\mathbf{n}}$ with $\mathbf{p} - (L/r) \hat{\Phi}$ to cancel the first cross product with part of the second cross product. We then

have

$$\frac{\partial H_{SO}}{\partial L} = \delta_1 \frac{\mathbf{S} \cdot \hat{\mathbf{L}}}{r^3} + \frac{\delta_1 L}{r^3} \mathbf{S} \cdot \left[\left(\hat{\mathbf{n}} \times \frac{\partial \hat{\Phi}}{\partial L} \right) - \left(\hat{\Phi} \times \frac{\partial \hat{\mathbf{n}}}{\partial L} \right) \right]$$

Taking the cross products we have

$$\begin{aligned} \frac{\partial H_{SO}}{\partial L} &= \delta_1 \frac{\mathbf{S} \cdot \hat{\mathbf{L}}}{r^3} - \frac{\delta_1}{r^3} \mathbf{S} \cdot \cos \theta_L \left(\hat{\mathbf{k}} - \cot \theta_L \hat{\Psi} \right) \\ &= \delta_1 \frac{\mathbf{S} \cdot \hat{\mathbf{L}}}{r^3} - \frac{\delta_1}{r^3} \cos \theta_L \left(J - L_z - \cot \theta_L \mathbf{S} \cdot \hat{\Psi} \right) \end{aligned}$$

where in the last step we have used $\mathbf{S} \cdot \hat{\mathbf{k}} = J - L_z$. Taking $\mathbf{S} \cdot \hat{\Psi} = (\mathbf{J} - \mathbf{L}) \cdot \hat{\Psi} = -\mathbf{L} \cdot \hat{\Psi} = -L \sin \theta_L$ gives

$$\begin{aligned} \frac{\partial H_{SO}}{\partial L} &= \delta_1 \frac{\mathbf{S} \cdot \hat{\mathbf{L}}}{r^3} - \frac{\delta_1}{r^3} \cos \theta_L (J - L_z - L \cos \theta_L) \\ &= \delta_1 \frac{\mathbf{S} \cdot \hat{\mathbf{L}}}{r^3} - \frac{\delta_1 J}{r^3} \cos \theta_L \\ &= -\Omega_L \frac{L}{J} \end{aligned} \quad (\text{A37})$$

Added together Eqs. (A36) and (A37) give the equation of motion for Φ in Eqs. (28) as claimed. The Ψ equation can be derived similarly. Since both P_Φ and P_Ψ are constants, the Hamiltonian is cyclic in Φ and Ψ .

-
- [1] <http://www.ligo.caltech.edu>.
- [2] <http://www.lisa.nasa.gov>.
- [3] T. A. Apostolatos, C. Cutler, G. J. Sussman, and K. S. Thorne, *Phys. Rev. D* **49**, 6274 (1994).
- [4] L. Blanchet, A. Buonanno, and G. Faye, *Phys. Rev. D* **74**, 104034 (2006).
- [5] G. Faye, L. Blanchet, and A. Buonanno, *Phys. Rev. D* **74**, 104033 (2006).
- [6] P. Grandclement, V. Kalogera, and A. Vecchio, *Phys. Rev. D* **67**, 042003 (2003).
- [7] L. E. Kidder, *Phys. Rev. D* **52**, 821 (1995).
- [8] R. N. Lang and S. A. Hughes, *Phys. Rev. D* **74**, 122001 (2006).
- [9] A. Vecchio, *Phys. Rev. D* **70**, 042001 (2004).
- [10] F. Pretorius, *Class. Quant. Grav.* **23** (2006).
- [11] F. Herrmann, I. Hinder, D. Shoemaker, P. Laguna, and R. A. Matzner, *gr-qc/0701143* (2007).
- [12] M. Campanelli, C. O. Lousto, P. Marronetti, and Y. Zlochower, *Phys. Rev. Lett.* **96**, 111101 (2006).
- [13] J. G. Baker, J. Centrella, D.-I. Choi, M. Koppitz, and J. van Meter, *Phys. Rev. Lett.* **96**, 111102 (2006).
- [14] P. Marronetti et al., *Class. Quant. Grav.* **24**, S43 (2007).
- [15] M. A. Scheel et al., *Phys. Rev. D* **74**, 104006 (2006).
- [16] M. Campanelli, C. O. Lousto, Y. Zlochower, B. Krishnan, and D. Merritt, *Phys. Rev. D* **75**, 064030 (2007).
- [17] F. Pretorius and D. Khurana, *Class. Quant. Grav.* **24**, S83 (2007).
- [18] T. Damour, *Phys. Rev. D* **64**, 124013 (2001).
- [19] J. Levin and G. Perez-Giz, *Phys. Rev. D* **77**, 103005 (2008).
- [20] M. Boyle et al., *gr-qc/08044184* (2008).
- [21] M. Campanelli, C. O. Lousto, H. Nakano, and Y. Zlochower, *gr-qc/08080713* (2008).
- [22] I. Hinder, F. Herrmann, P. Laguna, and D. Shoemaker, *gr-qc/08061037* (2008).
- [23] B. Gong, *astro-ph/0401152* (2004).
- [24] C. Königsdoerffer and A. Gopakumar, *Phys. Rev. D* **71**, 024039 (2005).
- [25] Schäfer and Wex, *Phys. Lett. A* **174** (1993).
- [26] N. Wex and S. Kopeikin, *astro-ph/9811052* (1998).
- [27] M. D. Hartl and A. Buonanno, *Phys. Rev. D* **71**, 024027 (2005).
- [28] A. Buonanno, Y. Chen, and T. Damour, *Phys. Rev. D* **74**, 104005 (2006).
- [29] JL and RG.
- [30] H. Poincaré, *Méthodes Nouvelles de la Mécanique Céleste*, Gauthier Villars, Paris, 1892.
- [31] L. Wen, *Ap. J.* **598**, 419 (2003).
- [32] T. Damour and G. Schaefer, *Nuovo Cim.* **B101**, 127 (1988).
- [33] T. Damour, P. Jaranowski, and G. Schaefer, *Phys. Rev. D* **62**, 084011 (2000).
- [34] T. Damour, P. Jaranowski, and G. Schaefer, *Phys. Lett. B* **513**, 147 (2001).
- [35] T. Damour, P. Jaranowski, and G. Schaefer, *erratum-ibib.d* **63**, 029903 (2001).
- [36] P. Jaranowski and G. Schaefer, *erratum-ibib.d* **63**, 029902 (2001).
- [37] G. Schaefer, *Annals Phys.* **161**, 81 (1985).
- [38] N. J. Cornish and J. Levin, *Phys. Rev. Lett.* **89**, 179001 (2002).
- [39] N. J. Cornish and J. Levin, *Class. Quant. Grav.* **20**, 1649 (2003).
- [40] J. Levin, *Phys. Rev. Lett.* **84**, 3515 (2000).
- [41] J. Levin, *Phys. Rev. D* **67**, 044013 (2003).
- [42] S. Suzuki and K. ichi Maeda, *Phys. Rev. D* **55**, 4848 (1997).
- [43] X. Wu and Y. Xie, *Phys. Rev. D* **76**, 124004 (2007).
- [44] X. Wu and Y. Xie, *Phys. Rev. D* **77**, 103012 (2008).
- [45] A. Gopakumar and C. Königsdörffer, *Phys. Rev. D* **72**, 121501 (2005).
- [46] J. Levin, *Phys. Rev. D* **74**, 124027 (2006).
- [47] L. Barack and C. Cutler, *Phys. Rev. D* **69**, 082005 (2004).
- [48] K. Glampedakis and D. Kennefick, *Phys. Rev. D* **66**, 044002 (2002).
- [49] S. Drasco and S. Hughes, *Phys. Rev. D* **73**, 024027 (2006).
- [50] J. Levin, R. O'Reilly, and E. Copeland, *Phys. Rev. D* **62**, 024023 (2000).
- [51] K. Belczynski, R. E. Taam, V. Kalogera, F. A. Rasio, and T. Bulik, *astro-ph/0612032* (2007).
- [52] R. O'Shaughnessy, J. Kaplan, V. Kalogera, and K. Belczynski, *Ap. J.* **632**, 1035 (2005).